Chapter 2
Numerical Modeling and Simulations

Keywords Model attributes • Particle-fluid coupling • Two-fluid • Point-source • Direct simulation • Collisions • Coalescence • Boundaries

2.1 Multiphase and Particulate Modeling

The design of processes and equipment was traditionally accomplished in the past by experimentation, construction of prototypes, and the building of pilot plants. These methods have been time-consuming and labor-intensive and, in the beginning of the twenty-first century, have been proven to be very expensive. In the last two decades, modeling and computer simulations are increasingly used for the design of equipment and processes. The main advantage of computer simulations is that they require significantly less time and resources than the building, testing, and optimization of prototypes and pilot plants. The main disadvantage of simulations is that, oftentimes, the modeling does not accurately describe the actual engineering system to be built, and some or all the testing results suffer from inaccuracies. This appears to be a temporary drawback to the simulation methods because it is due to the fact that numerical simulations are recently developed methods in science and engineering. The art and science of simulations are in the early stages of development, and still, there is not a great deal of accumulated expertise on this subject. Such inaccuracies are related to lack of modeling knowledge or lack of understanding of physical phenomena associated with the systems or processes that are modeled. With the continuing research and the advancement of our knowledge of phenomena and systems to be simulated, the modeling techniques become better and the accuracy of the simulations continuously improves. In addition, the continuous improvements in computer algorithms and the increasing availability of more powerful computers and processing time will assist significantly the accuracy and reliability of simulations in the future.

E.E. (Stathis) Michaelides, *Heat and Mass Transfer in Particulate Suspensions*, SpringerBriefs in Applied Sciences and Technology,
DOI 10.1007/978-1-4614-5854-8_2,

The numerical simulation of systems and processes involves two stages:

(a) The modeling of the system or process by a set of equations, which are the governing and closure equations. The set ideally includes all the salient parts and features of the system or process and their interactions.
(b) The numerical implementation to obtain the solution of the governing equations. This includes the discretization of the set of equations and the numerical method to be followed in order to derive the solution.

From the beginning, it must be noted that a numerical model is a mathematical idealization of the system and not an exact replica of the system. The modeling will not replicate faithfully all the features of the system. However, a useful and "successful" model will faithfully reproduce the most important features, which are of interest to the modeler. The basic premise of the model is to provide reasonably accurate answers for the behavior of the system under different conditions. Therefore, the modeling process has to start with the inquiries that need to be answered for the modeled system. Some of these inquiries that are pertinent to particulate heat transfer systems are:

1. Is there an interest in the transient behavior of the system/process or is steady-state representation sufficient?
2. Is there an interest in the inhomogeneities of the distribution of particles or a space-averaged description is sufficient?
3. Is the system diluted—are the particles sparsely distributed—for the interactions of the particles to be neglected?
4. Does the system generate turbulence? Are the turbulence effects important for the system or process?
5. Is there a need to describe the motion and heat transfer from individual particles or a general/average description is adequate?
6. Are electrical or magnetic effects important to be modeled?
7. Are other effects important and need to be modeled?

Answers to these questions always assist in the modeling of the particulate system and guide the modeling and simulation processes. For example, if the answer to question 4 is negative, the modeling may be simplified considerably by the choice of laminar governing equations for the momentum and heat transfer. If the answer to this question is positive and turbulence is generated in the system, the modeler must use one of the several available turbulence models in order to accurately describe the turbulence in the carrier fluid flow. At this stage the modeler will have to decide how to include the particle–turbulence interactions in the model as one-way interaction or two-way interaction. In the latter case, the following two interactions will have to be modeled:

(a) Particles are dispersed by the turbulence field, and their motion and energy transfer are affected by the turbulent eddies.
(b) Particles modulate the carrier fluid turbulence and by extent, the velocity field of the carrier fluid.

It is apparent that the inclusion of both effects will increase the complexity of the model and the computational resources it requires. The advantage from the increased complexity is that the results of the model will be more accurate.

2.1.1 Desired Attributes of Models

A mathematical model is a set of equations that describes an actual system or process. Models are mathematical and often idealized representations of physical situations, not exact replicas of them. Therefore, a model may predict with a certain degree of accuracy the effects of some of the variables associated with a system or a process, but may not be capable to predict other parameters or, in extreme and undesirable cases, may even yield inaccurate predictions. For a model to be useful to engineers, whose function is to design or evaluate systems and processes, it is desirable to possess the following attributes:

1. Simplicity in the structure of its equations.
2. Use of well-defined parameters that are universally accepted.
3. Ease in its comprehension by the engineer or practitioner.
4. Accuracy, to the degree desired by the modeler, for the particular application and reliability for its predictions.
5. Computational robustness, simplicity in the coding of its elements, and relative simplicity of the required computational grid.
6. Generality in its applications. There is invariably a trade-off between generality and simplicity.
7. Clear path to the validation and verification of its results, by corroborating its predictions with parameters, which are readily and accurately measured in real applications of the model.
8. Completeness in computing all the needed parameters.
9. Correct asymptotic behavior when its results are extended to single-phase flows and energy transfer or to flows where the multiphase mixture is expected to behave as a single-phase fluid, such as very dilute bubbly systems or a dilute mixture of air with aerosol particles.
10. Agreement of the results with the empirical correlations that have been experimentally validated in the past and continue to be used in the design of processes and equipment.

Because some of the first applications of multiphase flows were in the design of industrial equipment related to boiling, condensing, refining, and heat exchange between fluids, the first simplified multiphase flow models were developed for pipe flows. The origin of these models is the area-averaged equations for a multiphase mixture (Delhaye 1981; Michaelides 2003) with several simplifications being made in order to facilitate closure and ease in computations. Delhaye (1981), Boure and Delhaye (1982), Wallis (1963), and Ishii (1975, 1990), among many others, have presented accounts of several of these models. In the sections that follow, the basic

features and equations of models for the flow and energy transfer from particulate systems will be presented. Some of the numerical methods that are used to obtain the numerical solution of the governing equations will also be briefly exposed.

2.2 Classification of Particulate Flows

The first method of the classification of particulate flows is related to the volumetric composition of the particle–fluid mixture in *dilute* and *dense* flows. Dilute flows occur at volumetric concentrations, ϕ, less than 2%, and dense flows occur in general at $\phi > 6.5\%$. Interparticle collisions and particle interactions must always be taken into account in dense flows, while the two phenomena may be neglected in dilute flows without significant loss of accuracy. In the *intermediate* range $2\% < \phi < 6.5\%$, modeling of the collisions and interactions depends on the degree of the desired accuracy to be achieved by the numerical scheme to be employed.

The value of 6.5% concentration stems from the average interparticle distance: If the particulate phase is composed of spheres with a uniform diameter, $d = 2\alpha$, in the dense flow regime, the average distance between two spheres is less than one sphere diameter, when $\phi > 6.5\%$. This implies that hydrodynamic interactions between the spheres, and interparticle collisions, may not be neglected. In general, particles—this term includes both solid particles and liquid drops—interact with the carrier fluid by exchanging mass, momentum, and energy. The most important classification of particulate flows for modeling purposes is done according to the type and strength of these interactions, processes that are often called the *coupling*, between the carrier phase and the particulate phase. Accordingly, we have the following four classifications of particulate flows.

2.2.1 One-Way Coupling

This type of particulate flows assumes that the carrier flow field affects the motion of the particles through the hydrodynamic drag force, but the particles exert a negligible effect on the carrier fluid. One-way coupling implies that there is very low volumetric concentration of particles and these particles have a negligible effect on the flow of the carrier phase. The particles move independently within the carrier fluid and exchange momentum and energy with the fluid based on the drag and heat transfer expressions for single particles. Interactions between particles are neglected. This type of flow is modeled by solving separately for the velocity and temperature fields of the carrier fluid in the absence of particles and following individual particles in a Lagrangian frame of reference with origin the center of the particles. Oftentimes these simulations are called *Monte Carlo* (*MC*) simulations. Typical examples of one-way coupling are the dilute pneumatic conveying or drying of particles, and heat transfer with nanofluids at very low volumetric concentrations.

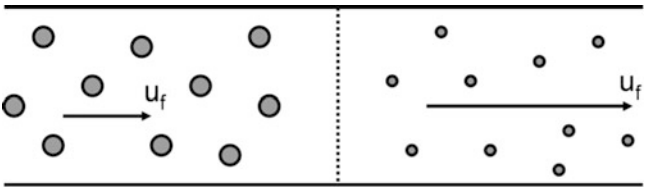

Fig. 2.1 Two-way coupling: The evaporation of drops in the two sections of this pipe causes the increase in the fluid volume and fluid velocity, which affects the transport velocity and heat transfer of the drops

2.2.2 Two-Way Coupling

In two-way coupling, the interactions of particles and carrier fluid are such that the effect of the interactions on the fluid may not be neglected, even though the volumetric flow of the particles is very low. A typical example of two-way coupling is the evaporation of drops in the last stages of boiling, which is depicted schematically in Fig. 2.1. Heat is transferred to the conduit, reaches the drops through the fluid, and causes their evaporation. Because the density of the drops is much larger than that of the produced vapor, the relatively small volume of the evaporating drops causes a significant increase in the volumetric flow of the vapor, which in a confined conduit accelerates significantly both fluid and drops.

Particles affect the carrier fluid in all chemical reactions where a vapor or gas is produced, including all combustion processes. Typically, in two-way coupling, the effects of the particles on the velocity and temperature of the carrier fluid are modeled as source terms in the mass, momentum, and energy equations. The motion of the individual particles or groups of particles may still be modeled in a Lagrangian way.

2.2.3 Three-Way Coupling

In addition to the effects of the carrier fluid on the particle motion and of particles on the fluid motion, in three-way coupling the hydrodynamic interactions between the particles, such as drafting in the wakes of preceding particles and lubrication effects, play an important role and are modeled. Also modeled are thermal interactions between particles, especially radiation heat transfer in combustors. Particles that produce heat, which is transferred to the surrounding fluid, induce a natural convection flow field around them. This field affects the velocity and temperature of the fluid and of other particles in the immediate vicinity. In the case of burning/reacting particles, the flow field emanating from the gases produced and the natural convection around particles is strong and must be modeled in a

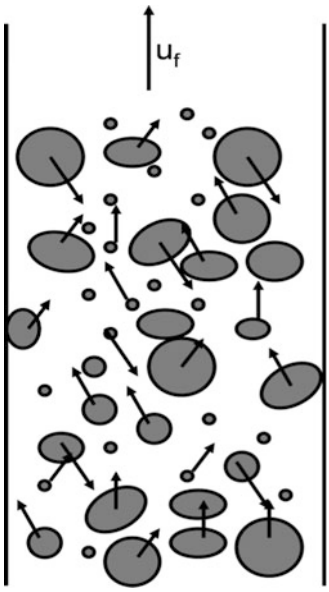

Fig. 2.2 Schematic diagram of a system, where modeling with four-way coupling is necessary

three-way modeling. Most applications of particulate systems with intermediate and dense concentrations, where combustion or evaporation occurs, are best to be modeled with a three-way coupling.

2.2.4 Four-Way Coupling

The modeling of interparticle collisions is the fourth element that characterizes the four-way coupling and is typically associated with dense flows. In a four-way coupling, the carrier fluid influences the motion and heat transfer from particles, and the particles affect the velocity and temperature of this fluid. In addition, the modeling takes into account the hydrodynamic interactions between the particles, particle–particle collisions, and particle–wall collisions. The flow and heat transfer in a fluidized bed reactor (FBR) as well as in most chemical reactors are typical examples, where four-way coupling is needed for the accurate modeling of the processes. Figure 2.2 is a schematic diagram of the velocities of particles in a FBR, where four-way coupling must be used for complete and accurate modeling. The velocities of several particles are shown by the representative vectors, $v(t)$. The velocity of the fluid is variable in space and time, $u_f = u_f(x_i,t)$, and equal to the particle velocity at each fluid–particle interface. It is apparent from this figure that hydrodynamic interactions occur between several particles as well as between groups of particles. The instantaneous velocities of the particles imply that several collisions are very likely to occur within a short time between particles as well as between several particles and the surrounding walls. The accurate and meaningful

description of the mass, momentum, and energy transfer in this system necessitates the accurate modeling of the fluid–particle, particle–fluid, and particle–particle hydrodynamic and energetic interactions, as well as the modeling of collisions between particles and between particles and surrounding walls. The four-way coupling is typically carried out numerically by the Eulerian description of the two phases, which is sometimes referred to as the *two-fluid model*. Closure equations for all the interactions must be supplied to the two-fluid models. The closure equations may be derived from experimental data, analytical studies, or more detailed numerical studies.

2.3 Modeling of the Carrier Phase: Governing Equations

In modeling the carrier fluid, one must first consider whether or not the carrier fluid domain may be characterized as a continuum. Flows and energy exchange in nanopores of membranes and chemical activation close to the surface of irregular catalyst particles are two examples where the molecular effects dominate and the carrier fluid in these regions may not be assumed to be a continuum. In most of the other applications of particulate heat transfer systems, the carrier fluid satisfies the continuum assumption. In this chapter, we will make use of the continuum assumption for the carrier fluid and will develop accordingly the governing equations for this fluid. Since most of the applications with particulates pertain to low Mach numbers, it will also be assumed that the carrier fluid flow is incompressible, that is, $\rho_f = \text{const}$. Hence, the mass conservation equation for the fluid—or continuity equation—becomes

$$\frac{\partial u_i}{\partial x_i} = 0 \quad \text{or} \quad \nabla \cdot \vec{u} = 0. \tag{2.1}$$

The form of the momentum and energy equations of the carrier fluid depends on whether or not flow instabilities have developed. The fluid Reynolds number, Re_L, which is based on the characteristic dimension of the carrier flow, L, plays an important role in the characterization and modeling of the carrier fluid flow. The flow is *laminar*, and the fluid does not develop any instabilities if $Re_L < Re_{cr}$, where Re_{cr} is the critical Reynolds number at which instabilities are initiated in the carrier fluid. Re_{cr} depends strongly on the geometry of the system that is modeled and its boundaries. The flow is *turbulent* if $Re_L > Re_{tu}$, where Re_{tu} is another higher number, beyond which the flow is fully turbulent. When $Re_{cr} < Re_L < Re_{tu}$, the flow has developed instabilities but is not fully turbulent and is called *transitional*. Because of lack of knowledge and more accurate modeling methods, transitional flows are frequently modeled in the same way as turbulent flows.

2.3.1 Laminar Flow

When $Re_{\mathrm{L}} < Re_{\mathrm{cr}}$, any instabilities that may be developed in the flow decay fast and the flow is stable. The time-dependent momentum and energy equations of the carrier fluid for laminar flow may be written as follows:

$$\begin{aligned} \rho_{\mathrm{f}}\left(\frac{\partial u_i}{\partial t}+u_j\frac{\partial u_i}{\partial x_j}\right) &= \rho_{\mathrm{f}} g_i - \frac{\partial P}{\partial x_i}+\mu_f\frac{\partial^2 u_i}{\partial x_j \partial x_j} \quad \text{or} \\ \rho_{\mathrm{f}}\left(\frac{\partial \vec{u}}{\partial t}+\vec{u}\cdot\nabla\vec{u}\right) &= \rho_{\mathrm{f}}\vec{g} - \nabla P+\mu_f\nabla^2\vec{u}, \end{aligned} \tag{2.2}$$

and

$$\begin{aligned} \rho_{\mathrm{f}} c_{\mathrm{f}}\left(\frac{\partial T}{\partial t}+u_j\frac{\partial T}{\partial x_j}\right) &= k_{\mathrm{f}}\frac{\partial^2 T}{\partial x_j \partial x_j} \quad \text{or} \\ \rho_{\mathrm{f}} c_{\mathrm{f}}\left(\frac{\partial T}{\partial t}+\vec{u}\cdot\nabla T\right) &= k_{\mathrm{f}}\nabla^2 T. \end{aligned} \tag{2.3}$$

For steady, laminar flow, the time-dependent terms vanish. In most applications, boundary layer approximations may be applied to appropriate regions of the system, e.g., near solid walls, which may simplify the stress tensor and the temperature gradients.

A special type of laminar flow is the *creeping flow* where $Re_{\mathrm{L}} \ll 1$. Under creeping flow conditions, the nonlinear advection terms, which appear in the left-hand sides of the last two equations, are very small in comparison to the other terms and may be neglected. In creeping flow, both momentum and energy equations become linear and may be solved analytically. Such flows occur in micro- and nano-channels as well as in the vicinity of fine particles. The solution of the creeping flow equations around spheres has resulted in many of the analytical expressions for the transient hydrodynamic force and transient heat transfer coefficients of spheres, which were presented in Chap. 1.

2.3.2 Turbulent Flow

When $Re_{\mathrm{L}} > Re_{\mathrm{tu}}$, the flow instabilities have been developed and have been sufficiently amplified in the flow domain to be distinct and to have caused the formation of vortices, local jets, and other flow structures, which persist over large ranges of timescales and lengthscales. The flow structures that develop in turbulent flows are unsteady, three dimensional, and span several lengthscales, from the large eddy scales, L_{LE}, to the Kolmogorov microscale, $L_{\mathrm{K}} = (\nu^3/\varepsilon)^{1/4}$. The latter is

considered the smallest scale of turbulent eddies. At the higher lengthscales, the flow structures are almost deterministic, but at the lower lengthscales, they are essentially stochastic. The momentum and energy equations of the carrier fluid for turbulent flow are the same time-dependent expressions written for the laminar flow regime [Eqs. (2.2) and (2.3)].

A complete numerical description of a turbulent flow field, with accurate representation of the large and small eddies, is possible, but it is computationally very demanding because the ratio of the large to small eddies, $L_{\mathrm{LE}}/L_{\mathrm{K}}$, is proportional to ${Re_{\mathrm{L}}}^{3/4}$. Simple calculations show that, for the simulation of water flow with velocity 1 m/s in a 5 cm pipe, $Re_{\mathrm{L}} \approx 50{,}000$ and $L_{\mathrm{LE}}/L_{\mathrm{K}} \approx 3{,}344$. A direct computation for this rather simple flow system would require at least 8,000 grid points in each direction or about 500 billion grid points, a significant computational resource. For this reason, averaging methods have been developed for the description of turbulence. Among these, the *Reynolds decomposition* stipulates that the turbulent velocities and temperature may be decomposed to a time-averaged and a time-dependent component as follows:

$$u_i(t) = \bar{u}_i + {u_i}'(t) \tag{2.4}$$

and

$$T(t) = \bar{T}_i + T'(t), \tag{2.5}$$

where u' and T' are the *fluctuating velocity* and *fluctuating temperature*, respectively, and the bar represents time averaging. Both of these variables have zero mean, and the standard deviation of the former is the turbulence intensity (Hinze 1975). The usual procedure to solve the governing equations is to substitute the fluctuating velocity and temperature in Eqs. (2.2) and (2.3), time average the resulting expressions, and solve for the time-averaged velocity and temperature fields. The substitution of the decomposed velocity and temperature into the governing momentum and energy equations yields an additional set of stresses, the *Reynolds stresses*, in the momentum equation as well as additional energy advection terms in the energy equation. In their final form, the time-averaged equations for turbulent flow and heat transfer are as follows:

$$\rho_{\mathrm{f}}\left(\frac{\partial \bar{u}_i}{\partial t} + \bar{u}_j\frac{\partial \bar{u}_i}{\partial x_j} + \frac{\partial \overline{u_i' u_j'}}{\partial x_j}\right) = \rho_{\mathrm{f}} g_i - \frac{\partial \bar{P}}{\partial x_i} + \mu_{\mathrm{f}}\frac{\partial^2 \bar{u}_i}{\partial x_j \partial x_j} \tag{2.6}$$

and

$$\rho_{\mathrm{f}} c_{\mathrm{f}}\left(\frac{\partial \bar{T}}{\partial t} + u_j\frac{\partial \bar{T}}{\partial x_j} + \frac{\partial \overline{T' u_j'}}{\partial x_j}\right) = k_{\mathrm{f}}\frac{\partial^2 \bar{T}}{\partial x_j \partial x_j}. \tag{2.7}$$

The first of the last two equations is often called the *Reynolds-averaged Navier–Stokes* (*RANS*) equation. It is used in the so-called *RANS models* for turbulence. The time-averaged terms in the last two equations are modeled by closure equations, which typically emanate from analysis, supplemented by experimental or other numerical data. Two simple closure equations for the two terms emanate from Prandtl's *mixing length* theory, which is often called the *zero-equation model* and has been very successful in modeling channel flows. The final expressions from the mixing length theory may be written as follows in the x, y, z system of coordinates (z is along the axis of symmetry of the channel flow):

$$\overline{u'_x u'_y} = \ell^2 \left|\frac{\partial \bar{u}_x}{\partial y}\right| \frac{\partial \bar{u}_x}{\partial y} = 0.41 y^2 \left|\frac{\partial \bar{u}_x}{\partial y}\right| \frac{\partial \bar{u}_x}{\partial y} \tag{2.8}$$

and

$$\overline{u'_x T'} = \ell^2 \left|\frac{\partial \bar{T}}{\partial y}\right| \frac{\partial \bar{u}_x}{\partial y} = 0.41 y^2 \left|\frac{\partial \bar{T}}{\partial y}\right| \frac{\partial \bar{u}_x}{\partial y}. \tag{2.9}$$

The last two expressions have been applied to turbulent boundary layer flows, such as the ones formed over flat plates and inside pipes and channels, and have produced accurate results. However, the equations have proven to be rather inaccurate when used with more complex, three-dimensional flows. For this reason, other turbulent models have been formulated, such as the *k–ε model* and three-, six-, or nine-equation models (Warsi 1993). Of these, the k–ε model and its several spinoffs are frequently used in most of the commercially available codes. These models use the concept of *eddy viscosity*, which is defined as

$$\mu_{\mathrm{T}} = C \rho_{\mathrm{f}} \frac{k^2}{\varepsilon}, \tag{2.10}$$

where C is a constant, with typical value $C = 0.09$; k is the kinetic energy of the velocity fluctuations, $k = 0.5\Sigma(u'^2_j)$; and ε is the rate of dissipation of the turbulent fluctuations. The k–ε model and similar models include two additional differential equations for the variables k and ε that need to be solved in conjunction with the Navier–Stokes equations (Warsi 1993).

The *large eddy simulation* (*LES*) method is often used in order to resolve for the larger vortices/eddies in the turbulence flow field. The LES method averages the smaller turbulent structures, especially those close to the boundaries. The LES method uses a decomposition of the velocity field that allows the larger eddies to be computed:

$$u_i(t) = \bar{u}_i + \tilde{u}_i(t) + u'_i(t), \tag{2.11}$$

with the second term representing the resolved large eddy structures, which are numerically computed. An averaging process similar to the k–ε model or simpler

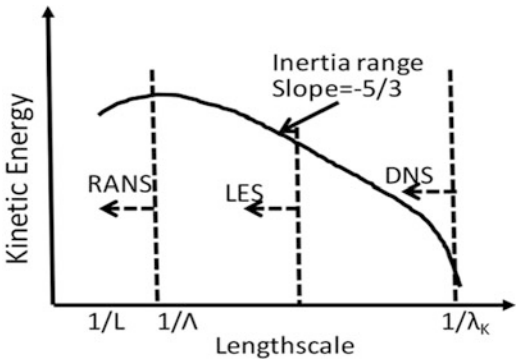

Fig. 2.3 Turbulent energy spectrum and computational capability of the RANS, LES, and DNS models. The *dashed arrows* indicate the ranges of the resolved lengthscales

algebraic models (Smagorinsky 1963) is used for the averaged stresses that emanate from the third term. The LES model gives a great deal of spatial and temporal information about the large flow structures that appear in engineering systems and has become a very promising and accurate computational technique in multiphase flows.

The *direct numerical simulation* (*DNS*) method solves the complete time-dependent Navier–Stokes equations and does not require a turbulence model. The *DNS* method, typically, resolves all eddy sizes and uses a very fine grid, which implies a high amount of computational resources. For most engineering computations at moderate or high Reynolds numbers, the fine grid requirement makes DNS computations prohibitive for large systems. Oftentimes, the detailed information provided by the DNS is also unnecessary for engineering design and optimization purposes. The main advantage of the DNS computations is that they are very accurate; they do not depend on assumptions or other closure equations and may be used to develop closure equations for the LES and RANS models.

Figure 2.3 is a diagram of a developed turbulent kinetic energy spectrum and the lengthscales resolved by each method for turbulence modeling. In this figure, L is the characteristic lengthscale of the engineering system, Λ is the turbulence integral lengthscale, and λ_K is the Kolmogorov microscale.

It must be noted that *hybrid* or combination methods, such as the RANS–LES method, have also been used in numerical applications. These methods are a compromise between the information gained by the solution of the model and the computational resources devoted to the solution.

For the determination of the heat transfer processes in most models, first, the velocity field is determined, and, secondly, the temperature field is computed using Eq. (2.7). The local heat transfer is then computed using the fundamental conduction equation, and the space-averaged heat transfer is computed by spatially integrating the local heat transfer.

2.3.3 *Transitional Flows*

Transitional flows are also characterized by velocity fluctuations, which start as two-dimensional and develop to become three dimensional. The turbulent flow structure is not well developed in transitional flows, and there is no apparent relationship and delineation between small and large eddies. Transitional flow is a difficult regime to simulate, primarily because a great deal is unknown in this regime. Both Eulerian models and Eulerian–Lagrangian models for the large vortices have been used in transitional flow simulations. In most of the engineering applications, transitional flows are modeled the same way as turbulent flows.

2.4 Modeling of Particulate Systems

Unlike other multiphase flow systems, where the phases flow in different and very complex regimes (e.g., bubbly, churn, or plug flow in gas–liquid systems), particulate flow systems are composed of dispersed particles or clusters of particles. For modeling purposes, the carrier fluid is always modeled as a continuum in an Eulerian way. The particulate phase or phases are modeled either in a Lagrangian or a Eulerian framework. An implicit condition that must be satisfied for the dispersed phase to be treated as a continuum in an Eulerian way is that the average interparticle distance must be significantly less than the size of the computational grid ($r_{ij} \ll \Delta x$). This imposes a lower limit on the flow features that may be resolved by the computational method and also implies that a large number of particles must be present in every cell of the grid. Figure 2.4 depicts two computational cells (a and b) where this implicit assumption is satisfied, one cell (c) where the continuum assumption is clearly not satisfied, and a fourth cell (d) which is a borderline case. If the Eulerian model were to be used for the description of the flow in cell (d), the computational results must be well validated.

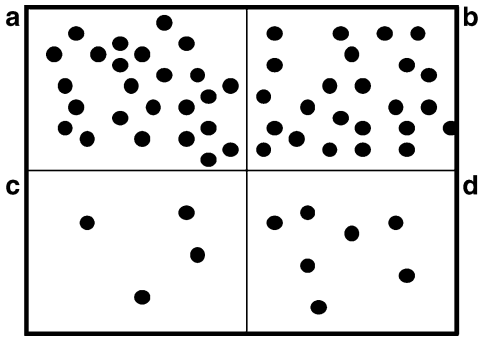

Fig. 2.4 Cells (a) and (b) have a sufficient number of particles for the particulate phase to be modeled as a continuum. Cell (c) may not be modeled as a continuum. Cell (d) is a borderline case: If the particulate phase in cell (d) were modeled as a continuum, in a Eulerian way, the results of the model would have to be well validated

2.4.1 Eulerian Homogeneous Model

A rather simple method to model a particulate system is to use the assumption that the fluid–particles mixture is homogeneous. The thermodynamic properties of the *homogeneous mixture* are given in terms of the volumetric fraction, ϕ, of the dispersed phase as follows (see Sect. 4.4 for more details):

$$\rho_{\mathrm{m}} = (1-\phi)\rho_{\mathrm{f}} + \phi\rho_{\mathrm{s}} \quad \text{and} \quad c_{\mathrm{m}} = \frac{1}{\rho_{\mathrm{m}}}[(1-\phi)c_{\mathrm{f}}\rho_{\mathrm{f}} + \phi c_{\mathrm{s}}\rho_{\mathrm{s}}]. \tag{2.12}$$

The momentum and energy equations for the homogeneous mixture become

$$\frac{\partial \rho_{\mathrm{m}} u_{\mathrm{m}i}}{\partial t} + \frac{\partial \rho_{\mathrm{m}} u_{\mathrm{m}j} u_{\mathrm{m}i}}{\partial x_j} = \rho_{\mathrm{m}} g_i - \frac{\partial P}{\partial x_i} + \mu_{\mathrm{m}} \frac{\partial^2 u_{\mathrm{m}i}}{\partial x_j \partial x_j} \tag{2.13}$$

and

$$\frac{\partial \rho_{\mathrm{m}} c_{\mathrm{m}} T_{\mathrm{m}}}{\partial t} + \frac{\partial \rho_{\mathrm{m}} c_{\mathrm{m}} u_{\mathrm{m}j} T_{\mathrm{m}}}{\partial x_j} = k_{\mathrm{m}} \frac{\partial^2 T_{\mathrm{m}}}{\partial x_j \partial x_j}. \tag{2.14}$$

It must be noted that the velocity u_{m} and temperature T_{m} are the space-averaged variables of the particulate mixture and that the two may be different than the corresponding variables of the carrier fluid and of the particulate phase. Also it must be noted that, while the thermodynamic properties of a mixture are well-defined as shown in Eq. (2.12), there is no agreement as to the definition of the transport properties of the mixture, μ_{m} and k_{m}. As will be further elaborated in Sect. 4.5, there is strong experimental evidence that the transport properties of the mixture depend on the distribution of the particles in the mixture. As a result, there is not a rigorous and accurate definition of μ_{m} and k_{m}. Modelers use ad hoc assumptions for the transport properties and, oftentimes, assume that they are equal to the corresponding properties of the carrier phase, μ_{f} and k_{f}. The epistemic uncertainty in the definition of the transport properties adds to the overall uncertainty of the computed results.

The homogeneous model is based on the average properties of the two phases and provides information only on these averages. It does not distinguish between particles and carrier fluid and does not answer questions, such as what is the relative velocity of the particles or what is the effect of the particulate phase on the overall heat transfer characteristics of the mixture. Because separate and more detailed information for the behavior of the two phases is desired, another Eulerian model, the two-fluid model, is often used for the modeling of particulate mixtures.

2.4.2 Eulerian, Two-Fluid Model

The *two-fluid* model, which is also called the *Eulerian point-source* model, treats the carrier fluid and the particles as two distinct continua that occupy the same volume. The two continua are governed by their own conservation equations (mass, momentum, and energy). The interactions of the two continua are modeled by source terms, which are added to the governing equations. For example, the momentum equation of the carrier fluid contains an additional force term that represents the drag exerted by the particles on this fluid. Similarly, the mass and energy conservation equations of the carrier fluid include terms that represent the sublimation/evaporation of particles and the energy transfer from the particles to the fluid, respectively. These terms need to be modeled, and typically, empirical equations are used for their modeling. The complete system of equations for the point-source model, applied to Newtonian fluids, is as follows:

A. Mass conservation for the fluid and the particulate phase:

$$\frac{\partial[(1-\phi)\rho_{\mathrm{f}}]}{\partial t}+\frac{\partial\left[(1-\phi)\rho_{\mathrm{f}}u_j\right]}{\partial x_j}=J. \tag{2.15}$$

$$\frac{\partial(\phi\rho_{\mathrm{s}})}{\partial t}+\frac{\partial\left(\phi\rho_{\mathrm{s}}v_j\right)}{\partial x_j}=-J. \tag{2.16}$$

B. Momentum conservation for the fluid and the particulate phase:

$$\frac{\partial[(1-\phi)\rho_{\mathrm{f}}u_i]}{\partial t}+\frac{\partial\left[(1-\phi)\rho_{\mathrm{f}}u_ju_i\right]}{\partial x_j}=(1-\phi)\left[\rho_{\mathrm{f}}g_i-\frac{\partial P}{\partial x_i}+\mu_{\mathrm{f}}\frac{\partial^2u_i}{\partial x_j\partial x_j}\right]+F_i+Jv_i. \tag{2.17}$$

$$\frac{\partial(\phi\rho_{\mathrm{s}}v_i)}{\partial t}+\frac{\partial\left(\phi\rho_{\mathrm{s}}v_jv_i\right)}{\partial x_j}=\phi\left[\rho_{\mathrm{s}}g_i-\frac{\partial(P+P_{\mathrm{c}})}{\partial x_i}+\mu_{\mathrm{s}}\frac{\partial^2v_i}{\partial x_j\partial x_j}\right]-F_i-Jv_i. \tag{2.18}$$

C. Energy equation for the fluid and the carrier phase:

$$\frac{\partial[(1-\phi)\rho_{\mathrm{f}}c_{\mathrm{f}}T_{\mathrm{f}}]}{\partial t}+\frac{\partial\left[(1-\phi)\rho_{\mathrm{f}}c_{\mathrm{f}}u_jT_{\mathrm{f}}\right]}{\partial x_j}=(1-\phi)k_{\mathrm{f}}\frac{\partial^2T_{\mathrm{f}}}{\partial x_j\partial x_j}+q. \tag{2.19}$$

$$\frac{\partial(\phi\rho_{\mathrm{s}}c_{\mathrm{s}}T_{\mathrm{s}})}{\partial t}+\frac{\partial\left(\phi\rho_{\mathrm{s}}c_{\mathrm{s}}v_jT_{\mathrm{s}}\right)}{\partial x_j}=\phi k_{\mathrm{s}}\frac{\partial^2T_{\mathrm{s}}}{\partial x_j\partial x_j}-q. \tag{2.20}$$

The mass source term, J, represents the mass transferred to the carrier fluid from the particles as a result of evaporation, sublimation, or chemical reactions.

The same term multiplied by the particle velocity appears in the momentum equations to represent the momentum transferred as a result of this mass exchange between the phases. In addition, the force term, F_i, also appears in the momentum equations to represent the hydrodynamic force between fluid and particles, such as drag and lift. Finally, the heat source term, q, represents the entire enthalpy transfer per unit volume from the particles to the carrier fluid and includes the latent heat of evaporation or sublimation, h_{fg}. The pressure term, P_{c}, represents the particle collisions and may be neglected if collisions are unimportant. It must be noted that terms, which are typically of significantly lesser orders of magnitude, such as the viscous dissipation term, have been omitted from the energy equation of the carrier fluid. As with the homogeneous model, the transport coefficients of the particulate phase, k_{s} and μ_{s}, have been assumed to be constant and need to be defined from empirical expressions. Oftentimes, these terms are assumed to be equal to the corresponding transport coefficients of the carrier fluid.

The equations in the point-source or two-fluid model are an extension of the governing equations of Newtonian fluids. As such, the system of equations of the model is robust and may be solved numerically by several of the algorithms that have been developed for the single-phase CFD. The accuracy of the model depends very much on the accuracy of the closure equations that are used for the interaction terms and the transport coefficients. For this reason, a great deal of computational and experimental work is being done to refine the closure equations.

Another source of uncertainty for the two-fluid models is the specification of the particles–wall boundary conditions that apply to the PDEs of the particulate phase: While the no-slip condition is routinely applied to solid walls as an accurate and time-tested boundary condition for fluids, it is not intuitive that the boundary condition for the solid phase should also be the no-slip condition. Actually, several experimental and DNS numerical studies have proven that there is significant slip of the particulate phase at the solid boundaries (Davis et al. 2011). The wall slip has to be given by a closure equation that is produced from experimental data or detailed computations. Two complications related to the specification of the particles–wall boundary condition are:

(a) The boundary condition for the particulate phase is defined at the plane where the centers of the particles are located when in contact with the wall. For spherical particles, this distance is one radius from the wall. Again, if particles of several sizes are present, or if the shapes of the particles are nonspherical, it is not clear where exactly the boundary condition for the solid phase should be applied. One way to address the second difficulty is to define several particulate phases, one phase for each size of particles (Mostafa and Elghobashi 1985). In the case of the continuous distribution of particle sizes, the phase may be defined for a range of sizes. While this practice may simplify the application of the boundary conditions, it increases significantly the number of PDEs that are to be solved, and if many phases need to be defined and their variables computed, the method becomes impractical.

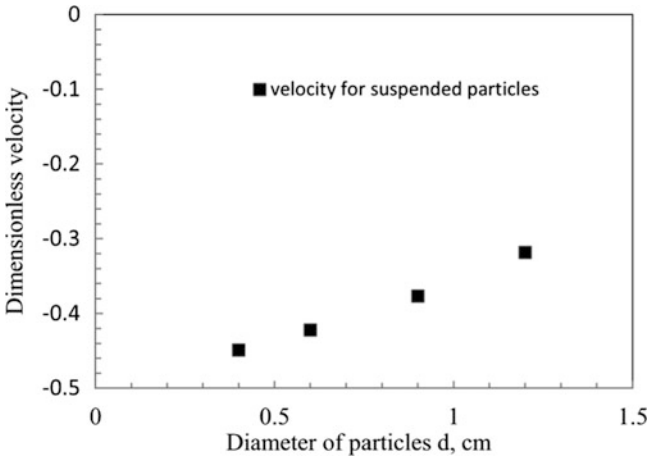

Fig. 2.5 Dimensionless vertical velocity of spherical particles at the plane where the boundary condition is defined

(b) The particle wall slip depends on the size of the particles. When the particulate phase is composed of particles with different sizes and shapes, it is neither known nor is it intuitive at all, what is the form of the velocity slip function at the solid boundary. As may be seen in Fig. 2.5, which depicts the dimensionless vertical velocity of particles at a plane one radius away from a vertical solid boundary, the particle slip at the vertical wall is finite and depends on the size of the particles. This difficulty may be addressed by conducting appropriate experimental or computational (DNS) studies near walls that will yield meaningful and reliable boundary conditions for the particulate phase.

2.4.3 Lagrangian, Point-Source Model

When dealing with discrete particles, it is more intuitive and physically meaningful to use a Lagrangian description with the center of coordinates at the center of gravity of the particles. The Lagrangian point-source models treat the particles as points that move in the flow field and are sources of mass, momentum, and energy for the fluid. The carrier fluid is treated as a continuum in an Eulerian way, and the velocity and temperature fields for the fluid are obtained from the solution of the PDEs in Eqs. (2.15), (2.17), and (2.19). The particle trajectories and temperatures are obtained by the solution of the ODEs, which emanate from the equation of motion and energy for particles:

$$m_{\mathrm{s}} \frac{\mathrm{d}v_i}{\mathrm{d}t} = \sum \left(F_{\mathrm{B}i} + F_{\mathrm{S}i} + F_{\mathrm{C}i} \right) \tag{2.21}$$

and

$$m_s c_s \frac{dT_s}{dt} = \sum \dot{Q}. \tag{2.22}$$

The forces in Eq. (2.21) include the body force, F_B, and surface or hydrodynamic force, F_S, on the particles as well as any interaction or collision forces with other particles and with the boundaries, F_C. Among the components of the hydrodynamic force are the steady drag, the added mass, the history, and the lift force, which are given in more detail in Sect. 1.3.6. Similarly, for the heat transfer, $\dot{Q}$, the steady convection as well as the history term must be included as described in Sect. 1.4.4. When the particles are considered as points, the angular momentum equation becomes meaningless. However, within the analytical framework of this model, particles of finite size may be considered. In this case, the angular momentum equation for the particles becomes:

$$I_p(\rho_s - \rho_f)\frac{d\omega_k}{dt} = -\rho_f \int_S e_{ijk}\left(x_j - x_{cj}\right)(F_{Sk} + F_{Ck})dS, \tag{2.23}$$

where the integral is computed around the surface of the particle and includes the friction forces; the tensor e_{ijk} defines the vector product (cross product) in the system of coordinates, i,j,k; and the point x_c represents the center of the particle. If the surface forces on the particle are given in terms of closure equations, this integral is equal to the sum of all the cross products of forces and the positions of the points of application.

The solution of the set of Eqs. (2.21), (2.22), and (2.23) is accomplished on a Lagrangian system of coordinates that follows the centers of the particles, usually by a time-marching method. For large numbers of particles, computational "parcels" are often used. Each parcel represents a number of particles with the same characteristics, such as shape, size, and density. A computational restriction in this case is that the size of the entire parcel should be smaller than the size of the computational grid.

For intermediate and dense flows, particle collisions play an important role in the determination of the trajectories of particles. Simple, deterministic collision models that emanate from first principles (momentum conservation and partial mechanical energy dissipation during the collision) are not sufficiently accurate to describe the particle interactions, especially where nonspherical particles and particles of different sizes are present. For this reason, probabilistic collision models have been proposed and are being used. The collision models are examined in more detail in Sect. 2.4.6.

The Lagrangian, point-source model is robust and relatively easy to implement, especially when the particle motion and energy exchange does not significantly influence the velocity and temperature fields of the fluid. A special case of the application of the model is the so-called *Monte Carlo* (*MC*) *simulations*, which were originally developed to simulate the effects of fluid turbulence and

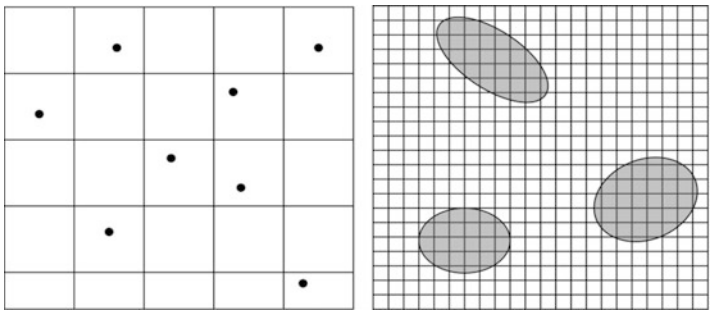

Fig. 2.6 The point-source model may handle a large number of particles, which must be smaller than the size of the grid. The resolved-particle model may only handle a small number of particles, and its grid must be significantly smaller than the size of the particles

time-varying temperature fields on the motion of particles (Gosman and Ioannides 1983) and on the heat transfer of particles (Michaelides et al. 1992). With MC simulations, the average carrier fluid velocity and temperature fields are first solved assuming there are no particles. Secondly, a probabilistic approach to model the velocity and temperature fluctuations of the fluid is used, typically from a known random distribution. A large number of particles are inserted in the flow field, and their momentum and heat exchange with the carrier fluid are computed using Eqs. (2.21), (2.22), and (2.23). The ensemble average of all the particles is computed. According to the ergodic hypothesis, the ensemble-averaged properties are equal to the time-averaged properties of the particles.

The drawback of the simple MC simulations is that the effects of the particles on the fluid velocity and temperature fields, as well as the particle–particle interactions, are inherently neglected. The way the method is commonly applied renders the model a one-way interaction model. Because of this, MC simulations may be applied only to dilute flows and only give a qualitative representation of the average behavior of particles in denser flows or in flows where some regions have higher particle concentrations.

2.4.4 Lagrangian, Resolved-Particle Model

This is the type of model used in direct numerical simulations (DNS). In the resolved-particle model, the details of the solution of the carrier phase velocity and temperature fields are such that it is feasible to determine the particle–fluid interactions from first principles. In this model the carrier phase numerical grid size is significantly smaller than the size of the particles ($\Delta x \ll \alpha$). Figure 2.6 contrasts the carrier phase grid size of this model with that of the point-source model. It is apparent that the resolved-particle model requires significantly higher computational resources for comparable numbers of particles. The solution of the carrier phase governing equations determines the pressure, velocity, and temperature fields around each particle. The mass flux, the hydrodynamic surface force, and the rate of

heat transfer between each particle and the fluid may be determined by integrating the concentration, stress, and temperature gradient fields over the surface of the particles, A_p, as follows:

$$J = \int_{A_s} \rho_v D_{vf} \frac{\partial c_v}{\partial x_j} n_j dA_s \tag{2.24}$$

where D_{vf} is the diffusion coefficient of the vapor stemming from the particles in the carrier fluid because of sublimation or evaporation; ρ_v is the vapor density; c_v is the volumetric concentration of the vapor in the carrier fluid; and n_j represents the outward normal vector to the particle surface, A_s. The hydrodynamic force is calculated from the expression:

$$F_{s,i} = \int_{A_s} \left[-P\delta_{ij} + \mu_f \left(\frac{\partial u_i}{\partial x_j} + \frac{\partial u_j}{\partial x_i} \right) \right] n_j dA_s \tag{2.25}$$

where δ_{ij} is the Kronecker delta. Finally, the rate of heat that enters[1] the particle is

$$\dot{Q} = \int_{A_s} \left(-k_f \frac{\partial T_f}{\partial x_j} \right) n_j dA_s. \tag{2.26}$$

The equation for the rotational motion of the particle in this model is the same as Eq. (2.23). Under this model there is no need for closure equations to account for the particle–fluid interactions. Of course, the resolution of the fields around the particles and the condition $\Delta x \ll \alpha$ implies that a very fine grid must be used in the resolved computations. A great deal of computational resources must be used even when the motion and energy exchange from a moderate number of particles is considered. Because of this, the resolved method is not suitable when a large number of particles need to be simulated in the system. This precludes the application of the DNS model to large engineering systems, such as fluidized bed reactors, which contain a very large number (of the order of 10^{10}) of discrete particles. Actually, such detailed information on the behavior of individual particles is not necessary for the design of large engineering systems.

The main advantage of the resolved-particle or DNS model is that it does not require empirical closure equations for the fluid–particle interactions. These are determined from first principles. The only empirical information required by the resolved-particle model is related to the collision of the particles. With a suitable collision scheme, this model determines accurately the behavior of all particles. When the grid of this model is very fine, in order to provide high accuracy results

[1] In Eqs. (2.22) and (2.26) we follow the thermodynamic convention: Heat that enters the system (particle) is positive.

for the particle–fluid interactions, then the DNS model itself may be used for the development of other, needed closure equations of these interactions. This includes the development of closure equations for the drag and convective heat transfer coefficients, C_D and h_c, from certain irregularly shaped particles, for which closure equations are not currently available. Such closure equations for the fluid–particle interactions may be further used to improve the accuracy of the Eulerian and the point-source models, thus enabling the simulations of large number of particles and realistic engineering systems. Therefore, the detailed information obtained from the resolved-particle model may be used to provide accurate information that feeds into models for large-scale engineering systems, where global information is required and the behavior of individual, separate particles is not of interest.

2.4.5 The Probability Distribution Function Model

The probability distribution function (PDF) method has been developed to handle simultaneously the flow turbulence and the behavior of small particles in a turbulent flow field. The origins of this method are in the kinetic theory of gases and can be traced to the studies by Maxwell and Boltzmann. Probabilistic methods were developed for the dense flow or granular materials, where the behavior of the particulate system is dominated by the collisions (Jenkins and Richman 1985; Ding and Gidaspaw 1990). These models apply to dense particulate systems, where the volumetric fraction is higher than 10% and the influence of the interstitial gas on the particle transport properties is almost negligible. Seeking an extension to lower volumetric fractions and dilute particulate systems, several researchers developed similar approaches that are based on the PDF equations for particles with additional closure equations, which account for the mass transfer, the hydrodynamic force, the heat transfer, fluid turbulence, and interparticle collisions.

An integral part of the kinetic theory models is the existence of a general equation that contains, implicitly or explicitly, terms, which yield the continuum description of the underlying medium. In the case of the kinetic theory of gases, the general equation is the Maxwell–Boltzmann equation for the probability distribution of the molecular velocities. In the case of particulate mixtures, the general equation is the *PDF equation*. The characteristic of the general PDF equation is that it may yield by a formal mathematical way the continuum equations for the flow and heat transfer of the carrier gas and the particles and, also, the natural boundary conditions that are observed near the walls—the near wall behavior of particles. Several PDF equations and models have been developed in the 1990s and have been used successfully to derive continuum conservation equations for particulate turbulent flows and heat transfer. Morioka and Nakajima (1987), Reeks (1991), and Zaichik and Vinberg (1991) were among the first to propose PDF equations for the treatment of the statistical averages and the behavior of multiphase systems.

Let us consider the motion of a dilute particulate system, where the particles exchange mass momentum and energy with the carrier fluid. We will denote by $X(t)$

the phase-space vector of a single particle as it moves through the phase space. The phase space in this case has 8 dimensions—three for the position, three for the velocity, one for the instantaneous mass, and one for the instantaneous temperature—and may be written at the instant of time t formally as

$$X(t) = [\vec{v}, \vec{x}, m_s, T_s]. \tag{2.27}$$

The time derivative of the phase-space vector may be obtained explicitly:

$$\dot{X}(t) = \left[\dot{\vec{v}}, \dot{\vec{x}}, \dot{m}_s, \dot{T}_s\right] = \left[\dot{\vec{v}}, \vec{v}, \dot{m}_s, \dot{T}_s\right]. \tag{2.28}$$

The last equation implies that the phase-space vector contains implicitly or explicitly information on the equation of motion of the particles, the heat transfer equation, and the mass transfer equation of the particles in the carrier fluid.

In analogy with the kinetic theory of gases, the number of particles in an elemental volume of the phase space d^nX located at X will be given by the product of the phase-space density function, $W(X,t)$, and the elemental volume d^nX. The fundamental number conservation equation may be applied to the phase space, to yield the condition:

$$\frac{\partial W}{\partial t} + \frac{\partial}{\partial X}\left[W\dot{X}\right] = 0. \tag{2.29}$$

Because turbulence is developed in the carrier fluid, the time derivative of the phase-space vector, $\dot{X}(t)$, has a time-dependent component, which may be assumed to be random. Therefore, one may assume a number of realizations of the phase-space vector, $X(t)$, at a given instant of time t. One may take the *ensemble average* of all the realizations of the phase-space density function, W, which will be denoted as $<W>$. The equation for $<W>$ is the PDF equation of this problem and may be obtained by ensemble averaging the last conservation equation. In the case of the dilute system of particles considered here, one may decompose the result to write explicitly its PDF equation as follows:

$$\frac{\partial \langle W\rangle}{\partial t} + \left(\frac{\partial \langle \dot{m}_s\rangle}{\partial m_s} + \frac{\partial \langle \dot{T}_s\rangle}{\partial T_s} + \frac{\partial \vec{v}}{\partial \vec{x}} + \frac{\partial \left\langle \dot{\vec{v}}\right\rangle}{\partial \vec{v}}\right)\langle W\rangle + \frac{\partial \langle \dot{m}'_s W\rangle}{\partial m_s} + \frac{\partial \left\langle \dot{T}'_s W\right\rangle}{\partial T_s} + \frac{\partial \left\langle \dot{\vec{v}}' W\right\rangle}{\partial \vec{v}} = 0, \tag{2.30}$$

where it was recognized that $\vec{v} = \dot{\vec{x}}$.

It is apparent that the PDF equation must be supplemented with expressions for $\dot{m}_s$, $\dot{T}_s$, $\dot{\vec{v}}$, etc. Such expressions are generated from the equation of motion and the energy equation of single particles. For example, the expressions for the particle acceleration vector and the rate of temperature change for dilute particulate flows

may be obtained directly from the appropriate expressions in Sects. 1.3 and 1.4. For more details of this method of modeling and some of the results that may be obtained, Reeks and Simonin (2006) and Simonin (2001) provide excellent reviews on the subject.

2.4.6 Particle Collisions

Particle collisions are infrequent in dilute flows and for this reason are neglected. Collisions increasingly influence the motion and heat transfer of particulates with increasing concentration. Except in very dense mixtures with $\phi > 45\%$, particle collisions are considered *binary*. The term implies that collisions between more than two particles are infrequent enough to be neglected. This stipulation simplifies considerably the analytical treatment of the collision processes and the effects of the collisions on the transport properties of the mixture. When multiparticle collisions become dominant, as in very dense particulate flows, the flows are characterized as *granular flows*. Usually fluid–particle interactions and inertia effects are neglected in the treatment of granular flows.

Rigid particles collide and separate. Liquid drops may collide and either separate with no other change, or break up, or coalesce. In the last two cases, the collision process is dominated by the surface deformations and surface force effects. Interparticle collisions occur during a finite amount of time, which is, in general, much shorter than the characteristic times of the particles, τ_M and τ_{th}. During the short collision process, interaction forces are developed between the particles, which are by far greater than the hydrodynamic forces between the particles and the fluid. Depending on the surface properties and the type of collision, the particles may also slide at the contact surface. A sliding friction force is thus developed, which is normally modeled using Coulomb's friction law. Deformations of the surfaces of the particles occur during the collision process. In most cases, the deformations are assumed to be negligible in comparison to the interparticle distance. Therefore, the interparticle distance remains constant during the collision process, and the contact may be assumed to occur at a single point, where the interparticle force is applied.

Two mathematical models to describe the collisions of particles have been developed: the *hard-sphere model* and the *soft-sphere model*. In the hard-sphere model, the impulses of all the forces between the colliding particles are assumed to be constant and are given in an integral form. This model lumps all the effects of the collision process into a single variable: the impulse produced by the interparticle force during the entire collision process. In the soft-sphere model, the governing equations are given in differential form. The magnitude of forces and moments vary during the collision process. Newton's second law determines the particles' velocity changes due to these transient forces and moments.

Figure 2.7 shows schematically the hard-sphere collision process. The initial velocities of the particles are denoted by the subscript 0, and the impulse force, which is developed during the collision, is denoted as $\vec{F}$. Elementary mechanics

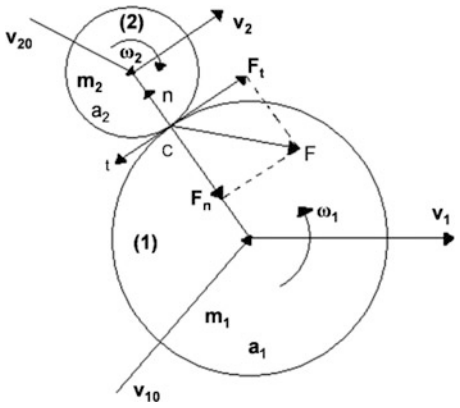

Fig. 2.7 Instantaneous forces between two colliding solid spheres

theory proves that the rectilinear and angular velocities of the two particles after the collision process are given by the following expressions:

$$\begin{aligned} m_1(\vec{v}_1 - \vec{v}_{10}) = m_2(\vec{v}_2 - \vec{v}_{20}) = -\vec{F} = \int_0^{\delta t} \vec{f}\,\mathrm{d}t \\ I_1(\vec{\omega}_1 - \vec{\omega}_{10}) = \alpha_1 \vec{n} \times \vec{F}, \quad I_2(\vec{\omega}_2 - \vec{\omega}_{20}) = \alpha_2 \vec{n} \times \vec{F}. \end{aligned} \tag{2.31}$$

It must be noted that $\vec{F}$ denotes the impulse of the all the forces acting on the particles during the entire duration of the collision time, δt. For spherical particles, the moment of inertia I is equal to $0.4\,\mathrm{m}\alpha^2$. Since the impulse of the force, $\vec{F}$, cannot be determined from the first principles of mechanics, the hard-sphere model for collisions makes use of the relative motion of the two particles and their material properties to derive expressions for the particle velocities at the end of the collision process. Let us decompose the impulse, $\vec{F}$, into two components: the first along the line of the centers of the two particles, which is normal to the surfaces at the point of contact, and the second in the perpendicular direction of the line between the centers, which is the tangential direction at the point of contact. Hence,

$$\vec{F} = F_\mathrm{n}\vec{n} + F_\mathrm{t}\vec{t}. \tag{2.32}$$

The normal relative velocities of the two particles, before and after the collision process, are related by a restitution coefficient, e_r:

$$\vec{n} \bullet (\vec{v}_1 - \vec{v}_2) = -e_\mathrm{r}\vec{n} \bullet (\vec{v}_{10} - \vec{v}_{20}) \quad \text{or} \quad \vec{n} \bullet \vec{w} = -e_\mathrm{r}\vec{n} \bullet \vec{w}_0. \tag{2.33}$$

From the last three equations, one obtains the following expression for the normal component of the impulse force:

$$F_\mathrm{n} = \frac{-m_1 m_2}{m_1 + m_2}(1 + e_\mathrm{r})(\vec{n} \bullet \vec{w}_0). \tag{2.34}$$

For the collision to occur, the normal component of the relative velocity of the particles must be in the direction of the vector $\vec{n}$. Hence, the last scalar (dot) product is positive. Since the restitution coefficient is also positive, the last equation implies that $F_n < 0$. Hence, the normal force is directed inward, that is, in the direction defined from the point of the collision to the center of the particle.

If the particles slide during the collision process and the coefficient of friction is denoted by f_f, then Coulomb's law of friction is applied ($F_t = f_f F_n$) to yield the tangential component. The condition for sliding to occur is (Crowe et al. 1998)

$$F_t > -\frac{2}{7}\frac{m_1 m_2}{m_1 + m_2}|\vec{w}_{0tc}| \quad \text{or} \quad \frac{\vec{n} \bullet \vec{w}_0}{\vec{w}_{0tc}} < \frac{2}{7 f_f (1 + e_r)}, \tag{2.35}$$

where the vector $\vec{w}_{0tc}$ is the initial tangential velocity at the point of contact.

Hence, the linear and angular velocities of the two particles after the sliding collision process are given by the following expressions:

$$\begin{aligned}
\vec{v}_1 &= \vec{v}_{10} - (\vec{n} \bullet \vec{w}_0)(1 + e_r)\frac{m_2}{m_1 + m_2}(\vec{n} - f_f \vec{t}\,) \\
\vec{v}_2 &= \vec{v}_{20} + (\vec{n} \bullet \vec{w}_0)(1 + e_r)\frac{m_1}{m_1 + m_2}(\vec{n} - f_f \vec{t}\,) \\
\vec{\omega}_1 &= \vec{\omega}_{10} + \frac{5}{2\alpha_1}(\vec{n} \bullet \vec{w}_0) f_f (1 + e_r)\frac{m_2}{m_1 + m_2}(\vec{n} \times \vec{t}\,) \\
\vec{\omega}_2 &= \vec{\omega}_{20} + \frac{5}{2\alpha_2}(\vec{n} \bullet \vec{w}_0) f_f (1 + e_r)\frac{m_1}{m_1 + m_2}(\vec{n} \times \vec{t}\,).
\end{aligned} \tag{2.36}$$

If the sliding motion stops during the hard-sphere collision process, the condition of Eq. (2.35) is not satisfied. In this case, at the end of the collision process, the relative velocity of the particles is zero, and the expressions for the particle velocities after the collision are

$$\begin{aligned}
\vec{v}_1 &= \vec{v}_{10} - \frac{m_2}{m_1 + m_2}\left[(1 + e_r)(\vec{n} \bullet \vec{w}_0)\vec{n} + \frac{2}{7}|\vec{w}_{0tc}|\vec{t}\right] \\
\vec{v}_2 &= \vec{v}_{20} + \frac{m_1}{m_1 + m_2}\left[(1 + e_r)(\vec{n} \bullet \vec{w}_0)\vec{n} + \frac{2}{7}|\vec{w}_{0tc}|\vec{t}\right] \\
\vec{\omega}_1 &= \vec{\omega}_{10} - \frac{5}{7\alpha_1}|\vec{w}_{0tc}|\frac{m_2}{m_1 + m_2}(\vec{n} \times \vec{t}\,) \\
\vec{\omega}_2 &= \vec{\omega}_{20} - \frac{5}{7\alpha_1}|\vec{w}_{0tc}|\frac{m_1}{m_1 + m_2}(\vec{n} \times \vec{t}\,).
\end{aligned} \tag{2.37}$$

The expressions for the velocities of the two particles at the end of the collision process may be used as closure equations to determine the effect of the collisions on the dynamics of a particulate mixture.

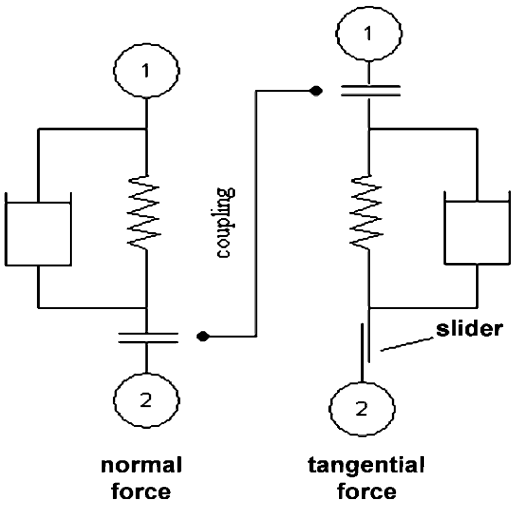

Fig. 2.8 Force model for soft-sphere collisions with friction

Figure 2.8 depicts the schematic diagram of the soft-sphere collision model. The basic premise of the soft-sphere model is that the interparticle force is variable during the collision process. This model calculates the instantaneous value of the collision force, using Newton's second law. The soft-sphere model presumes that the colliding particles overlap by a small distance, δ, which is very small in comparison to the particles' dimensions. The overlapping distance is decomposed into a normal, δ_{n}, and a tangential component, δ_{t}. These two components are calculated from the initial strength of the impact between the particles and the stiffness of the particles. The force model includes simple elements from solid body dynamics, such as springs, dash pots, friction sliders, rollers, and latches. The coupling between the normal and tangential components of the force is also depicted in the figure. The stiffness coefficient, k_{s}; the damping factor, η_{d}; and the friction factor, f_{f}, which may be calculated from the material properties of the particles, are inputs to this model and are used to determine the normal and tangential components of the instantaneous force. In the most general case, these material properties have different values in the normal and tangential directions and are expressed as functions of the Young's modulus, E_{Y}, and the Poisson ratio σ_{P} of the materials. Thus, the components of the interparticle force for two spheres of equal radii may be written by the following set of equations:

$$F_{\mathrm{n}} = -\frac{\sqrt{2\alpha}E_{\mathrm{Y}}}{3(1-\sigma_{\mathrm{P}})}\delta_n^{3/2} - \eta_{\mathrm{dn}}\vec{w}\bullet\vec{n} \quad \text{and}$$

$$F_{\mathrm{t}} = \frac{2\sqrt{2\alpha}E_{\mathrm{Y}}}{2(1+\sigma_{\mathrm{P}})(2-\sigma_{\mathrm{P}})}\delta_{\mathrm{n}}^{1/2}\delta_{\mathrm{t}} - \eta_{\mathrm{dt}}\left[\bar{w} - (\vec{w}\bullet\vec{n})\vec{n} + \alpha\left(\omega_i + \omega_j\right)\times\vec{n}\right]\bullet\vec{n} \tag{2.38}$$

$$\text{if } |F_{\mathrm{t}}| < f_{\mathrm{f}}|F_{\mathrm{n}}| \quad \text{or} \quad F_{\mathrm{t}} = -f_{\mathrm{f}}|F_{\mathrm{n}}| \quad \text{if} \quad |F_{\mathrm{t}}| > f_{\mathrm{f}}|F_{\mathrm{n}}|.$$

Cundall and Strack (1979) recommended the following expressions for the damping coefficients:

$$\eta_{\mathrm{dn}} = \sqrt{m_{\mathrm{s}} \frac{\sqrt{2\alpha} E_{\mathrm{Y}}}{3(1-\sigma_{\mathrm{P}})}} \quad \text{and} \quad \eta_{\mathrm{dt}} = \sqrt{m_{\mathrm{s}} \frac{2\sqrt{2\alpha} E_{\mathrm{Y}}}{2(1+\sigma_{\mathrm{P}})(2-\sigma_{\mathrm{P}})} \delta_{\mathrm{n}}^{1/2}}. \tag{2.39}$$

It must be noted that, according to the soft-sphere model, the interparticle force is instantaneous and that its numerical value varies during the collision process. The laws of mechanics are used in a differential form to determine the linear and angular velocity changes during the collision process. This is usually accomplished by a numerical method (Tsuji et al. 1993; Kartushinsky and Michaelides 2004). Also, both the hard- and soft-sphere models may be extended to multiparticle interactions, though this does not appear to be necessary for the modeling of discrete dispersed systems.

The collision models are developed independently of the larger computational models, e.g., a DNS or a two-fluid model, for the flow and heat transfer from particulate systems. When an interparticle or particle collision model becomes part of a larger computational model, it is important that the collision model does not disturb significantly the local characteristics of the larger numerical model. The disturbance might make the larger model numerically unstable. The sudden introduction of a large force locally, which accompanies the collision process, in both the hard- and soft-sphere models, may introduce computational instabilities in a larger numerical code. For this reason, in several numerical algorithms, the collision forces are introduced gradually and are often applied "gently" before the surfaces of the particles collide. In these algorithms, the collision models are modified so that a repulsive force starts acting on both particles when the interparticle distance or the distance of the particle from the wall is less than a predefined threshold distance, ζ, which is typically in the range $0.1\alpha < \zeta < 0.2\alpha$. Such a model has been proposed by Glowinski et al. (2001) and has been successfully used by several others including Feng and Michaelides (2004). According to this model, the repulsive force between two particles is given in terms of the distance between the centers of the two particles, $|x_i - x_j|$, by the following expression:

$$F_{ij}^{\mathrm{P}} = \begin{cases} 0, & |x_i - x_j| > \alpha_i + \alpha_j + \zeta \\ \frac{c_{ij}}{\varepsilon_{\mathrm{P}}} \left(\frac{|\vec{x}_i - x_j| - \alpha_i - \alpha_j - \zeta}{\zeta} \right)^2 \left(\frac{x_i - x_j}{|x_i - x_j|} \right), & |x_i - x_j| \le R_i + R_j + \zeta \end{cases}. \tag{2.40}$$

The parameter, c_{ij}, is the force scale, which for typical particulate systems is chosen to be equal to the buoyancy/gravity force on the particles. Of the other parameters, ε_{P} is the stiffness parameter for collisions, and α_i and α_j are the radii of the two particles. Glowinski et al. (2001) provided the justification and an extensive discussion on how to choose the stiffness and force parameters.

This collision technique allows particles to overlap even when the stiffness parameter c_{ij} is very large. The partial overlapping of particles will be significant when a large number of particles undergo a packing process, for example, in flow stagnation regions. The particles at the bottom, which have to bear the load of the particles above, will be subjected to the maximum overlapping, and this may distort the geometric characteristics of the computational domain. To counteract significant overlapping, one has to choose a higher value for the repulsive force when the collision scheme given by the above expression is used. To resolve this issue, Feng and Michaelides (2005) employed a new collision scheme that chooses the magnitude of the repulsive force by considering the following situations: Before the two particles contact, the repulsive force given by Eq. (2.40) is used; when the two particles start to overlap, a stronger spring force is applied. The latter is proportional to the overlapping distance of two particles and is significantly larger than the repulsive force with no overlapping. According to this approach, the collision force equation is modified to the following form:

$$F_{ij}^{\mathrm{P}} = \begin{cases} 0, & |x_i - x_j| > \alpha_i + \alpha_j + \zeta \\ \frac{c_{ij}}{\varepsilon_{\mathrm{P}}} \left(\frac{|x_i - x_j| - \alpha_i - \alpha_j - \zeta}{\zeta} \right)^2 \left(\frac{x_i - x_j}{|x_i - x_j|} \right), & R_i + R_j < |x_i - x_j| \le \alpha_i + \alpha_j + \zeta \\ \left(\frac{c_{ij}}{\varepsilon_{\mathrm{P}}} \left(\frac{|x_i - x_j| - \alpha_i - \alpha_j - \zeta}{\zeta} \right)^2 + \frac{c_{ij}}{E_{\mathrm{P}}} \frac{(\alpha_i + \alpha_j - |x_i - x_j|)}{\zeta} \right) \left(\frac{x_i - x_j}{|x_i - x_j|} \right), & |x_i - x_j| \le \alpha_i + \alpha_j, \end{cases} \tag{2.41}$$

where the parameter E_{P} is smaller than ε_{P} to ensure a much larger spring force, which will minimize the overlapping of the particles. The first term in the last equation is retained from Eq. (2.40) to ensure that the collision force will be continuous when the particles first touch. The advantage of this collision scheme is that it enables one to use a smaller repulsive force for particle sedimentation before the packing starts and a larger spring force that keeps the particles separated during the packing process, where a larger force is needed to keep the particles apart. This collision scheme may be used in dense as well as granular flows.

The modeling of particle collisions with a smooth wall may be accomplished in a manner similar to the interparticle collisions, by assuming that the wall is a very large particle. Either the hard- or the soft-sphere model may be used, and the conditions with $m_2 \gg m_1$ and $\alpha_2 \gg \alpha_1$ will yield the linear and angular velocities of the particle after the collision process. Alternatively, one may use the concept of the *image particle*. This is a second, fictitious particle, symmetrical with respect to the wall that moves with velocity, which is the image of the velocity of the particle (Glowinski et al 2001; Feng and Michaelides 2005). The fictitious collision between the two particles has the same effect as the collision with a solid wall.

A complication to the modeling process arises when the size of the particles is of the same order of magnitude as the wall roughness. Particles that approach a rough surface bounce in a direction that is determined by the local curvature and not by the

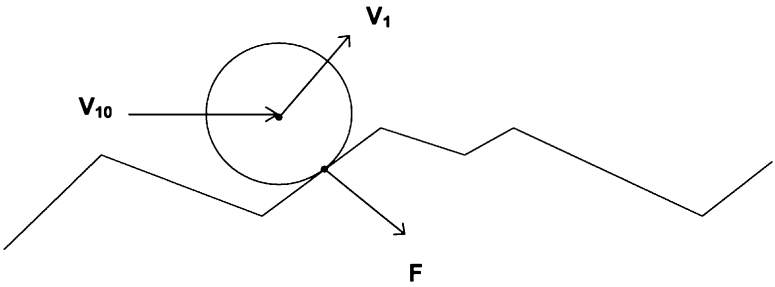

Fig. 2.9 Collision of a spherical particle with a rough surface—the reflection depends on the local geometry and not the overall shape of the surface

macroscopic shape of the surface. Hence, surface irregularities determine the direction of the bouncing particles as shown in Fig. 2.9. With collisions on a rough wall, it is neither possible nor desirable to simulate accurately the actual roughness of a wall surface. For this reason, statistical models for surfaces have been proposed that take into account the average features of the surface. These surface models use wavy patterns, random combinations of inclined planes, and random combination of pyramids and prisms (in three-dimensional simulations) arranged on a flat or rounded surface. Frank et al. (1993), Sakiz and Simonin (1999), Sommerfeld and Huber (1999), Sommerfeld (2003), and Taniere et al. (2004) have proposed such models for rough surfaces and used these models for particulate flow computations.

2.4.7 Droplet Collisions and Coalescence

Two viscous spheres, bubbles or drops, may coalesce when they are in close proximity or when they collide. The coalescence process is complex and depends on several variables including the size, surface tension, viscosity of the two phases, and the two velocity vectors (Manga and Stone 1993, 1995; Orme 1997). Most numerical methods do not handle coalescence from first principles and rely on closure equations and conditions for the entire process. Also, contrary to intuition, coalescence rarely occurs when two drops or bubbles interact (Qian and Law 1997). In most cases, when the paths of drops and bubbles intersect, the interaction causes collisions, which are similar to the collisions of solid particles, and separation at the end of the process. Experiments have shown that collisions between drops rarely occur in sprays, where the droplets move in almost parallel directions and that coalescence occurs only in dense regions, for example, near the orifice of an injector (Sirignano 1999).

Qian and Law (1997) conducted an extensive experimental study on the collision of two drops of equal size and showed that the behavior of the drops may be described in a plot of the Weber number, *We*, vs. the minimum dimensionless

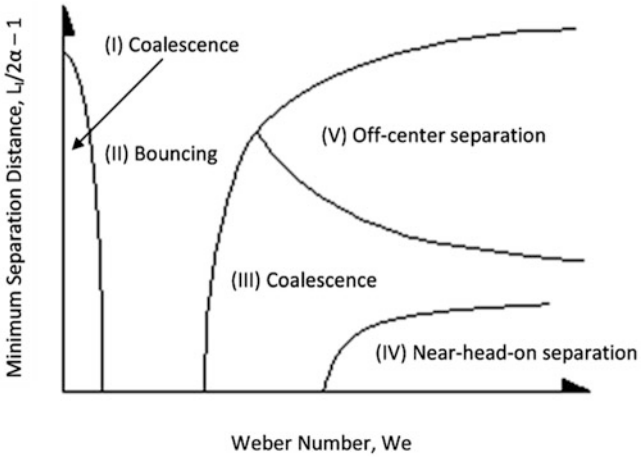

Fig. 2.10 Five coalescence regimes for the collision of two viscous spheres

separation distance, which is equal to $L_l/2\alpha - 1$. The outcomes of the collision process are two: coalescence or separation. The experimental results indicate that there are five distinct regimes for the collision process of the drops, three of which result in separation. The five regimes defined by Qian and Law (1997) are plotted qualitatively in Fig. 2.10. When two drops approach, the interstitial fluid between them stretches and becomes a thin film, with the pressure increasing locally. If the two drops approach slowly, the interstitial fluid film has time to drain, the surfaces of the drops touch, and coalescence occurs with minor deformation of the surfaces. This leads to collision regime I of Fig. 2.10, where the low values of We signify the low relative velocity of the drops. At higher initial relative velocity (higher We), the interstitial film does not have the time to drain, the higher pressure builds up quickly in the film, and the surfaces of the drops do not come in contact. The result is the deformation and repulsion/bouncing of the drops, which is depicted as regime II in Fig. 2.10. At even higher values of the relative velocity (and of We), the kinetic energy of the drops is high enough to forcibly expel the interstitial fluid film. The high kinetic energy also deforms substantially the two drops and finally causes their coalescence, as depicted in regime III. If the collisional kinetic energy of the drops is very high, the gaseous film is again drained, and the surfaces of the drops may touch temporarily. In this case, the system of the two drops has very high kinetic energy, which leads to vibrations and surface instabilities. The compound drop breaks up into two or more droplets. The experiments by Qian and Law (1997) distinguish two such regimes, denoted as IV and V in the figure, the first where the drops oscillate and undergo a reflective separation for a near head-on collision and the second where the drops stretch apart and undergo a stretching separation for off-center collisions.

Estrade et al. (1999) and Ashgriz and Poo (1990) provided a theoretical framework for the collision process of drops, which has resulted in analytical expressions for the description of the boundaries of regimes II and III, and of regimes III and IV.

Such analytical expressions, or the entire Fig. 2.10, may serve as closure equations in a numerical scheme for the determination of coalescence or separation. In the case of coalescence, the numerical computations continue by introducing a single drop in the computational domain and the colliding drops are taken off the computations. If the radii of the two colliding drops are α_1 and α_2, according to the volume conservation principle, the radius of the resulting drop after the coalescence, α_{12}, is

$$\alpha_{12} = \sqrt[3]{\alpha_1^3 + \alpha_2^3}. \tag{2.42}$$

Kollar et al. (2005) used these analytical results in a comprehensive model for the collision and coalescence of drops and determined the effects of these processes on the droplet size distributions. They concluded that the distribution of sizes of drops is affected significantly, not only by mass transfer processes, such as evaporation and condensation, but also by coalescence.

Of the computational schemes that may handle the coalescence of drops, the front/boundary-tracking method, which is described in more detail in Sect. 2.5.2 (Unverdi and Tryggvason 1992), has been developed to include surface tension forces and has been used to track bubbles and drops in viscous fluids. Nobari et al. (1996) also used this method to model the axisymmetric collisions of drops. Their computational results showed that the two drops deform significantly upon impact, and their fronts become flat. A very thin layer of the viscous interstitial fluid was retained between the two drops by the computational scheme, which did not have enough time to drain during the collision process. The presence of this fluid layer always caused the eventual rebounding of the drops. Coalescence in this computational scheme occurred only when the interstitial fluid layer was artificially drained using a specified condition in the numerical algorithm. The timing of the drainage process and the conditions under which the drainage of the film is applied take the place of the closure equations for the numerical method.

The study by Nobari et al. (1996) suggests that any assumptions made for the drainage of the interstitial fluid in all the numerical methods are crucial for the eventual coalescence or rebound of drops in a viscous fluid. Since for head-on collisions with significant pre-collision momentum, the minimum gap between the drops is composed of only a few molecular layers, computations at the molecular level may be needed to accurately determine the mechanics of the film drainage and the coalescence process of drops. This imposes the problem of modeling at the molecular and the continuum scales simultaneously, which is a rather challenging but not insurmountable task.

2.4.8 Heat Transfer During Collisions

The collision time is very short for all types of particles (this includes solid particles as well as drops). In addition, the area of contact between particles during the

collision process is also very small, for the conduction through that area to be significant. For this reason, the heat transfer between particles during an entire collision process is negligible in comparison to the heat exchanged between particles and fluid. The fluid and the particles continue to exchange energy during the collision processes. For a spherical particle, the rate of heat transfer is given in terms of the convective heat transfer coefficient, h_c, and the temperature difference as follows:

$$\dot{Q} = 4\pi\alpha^2 h_c \left(T_p - T_f\right). \tag{2.43}$$

The dependence of the convective heat transfer coefficient, h_c, on the proximity of other particles, or during the physical collision process when deformation occurs, has not been thoroughly investigated. Given that the duration of the collisions is very short in comparison to the thermal timescale of the particles, τ_{th}, the effects of the collisions on h_c (and by extent on Nu) are typically neglected. Hence, the closure equations for Nu, presented in Sect. 1.4, may be used during collisions. In general, the effect of interparticle collisions or particle collisions with walls influence primarily the velocity of the particles, and any effects on the energy exchange come through the dependence of h_c (or Nu) on the particle velocity. In the case of drop coalescence, the resulting drop that is introduced in the computational scheme after the coalescence continuously exchanges mass and heat with the carrier fluid according to the correlations presented in Sect. 1.4.

2.5 The Treatment of Particle Boundaries

Numerical computations are performed on the nodes of the numerical grid, which typically follow a geometric pattern. Solid and fluid boundaries of particles do not necessarily coincide with these nodes. Eulerian (two-fluid) models do not model the flow and energy exchange of individual particles and do not need to account for particle boundaries. On the other hand, DNS and similar models, which account for individual particles, must accurately describe the surface of the particles that are tracked. Among the techniques that have been used for the description of the surface of the particles are the following.

2.5.1 Body-Fitted Coordinates

In the Body-Fitted Coordinates (BFC) method, the numerical grid is constructed according to the shape of the particles. Spherical particles are more easily fitted to a spherical coordinate system, but particles of other shapes may also be fitted. Alternatively, a coordinate transformation may be made (Thompson et al. 1982)

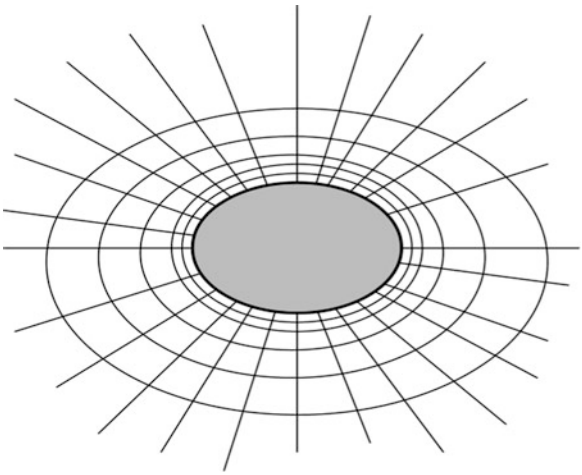

Fig. 2.11 Body-fitted coordinate system with an ellipsoidal particle

to fit the boundary of a particle to a coordinate system. If the particle shape is complex or irregular, this transformation may be accomplished numerically. Figure 2.11 shows an ellipsoidal particle fitted to a simple ellipsoidal system of coordinates. The no-slip boundary condition may be easily applied to the nodes, which describe the surface of this particle, by defining the velocity at these nodes to be equal to zero. Because the numerical grid needs to be denser close to the solid surface, oftentimes a logarithmic equation is used for the spacing of the grid nodes (Feng and Michaelides 2001). Any robust numerical scheme, such as finite difference or finite elements/volumes, may be used for the solution of the governing equations.

The BFC method is simple and ideal for the modeling of stationary, single particles, where the center of the coordinate system may coincide with the center of the particles. However, this method becomes cumbersome when several particles that are moving around are included in the computational domain. Some authors have counteracted this difficulty, by re-meshing after every time step, but this becomes computationally expensive (Patankar et al. 2001). Also, when particles are in close proximity to each other, a great deal of nodes is required to be used for the resolution of the interstitial fluid. This increases significantly the amount of computational resources that are necessary for the application of the method.

With boundary-fitted coordinates, typically, the equation of motion for the particles is solved first, and, secondly, the energy equation is computed to yield the heat transfer between the particles and the fluid. In the case of BFC, both the momentum and the energy equations for particles may be solved on the same numerical grid. Among the recent studies that used the BFC method are McKenna et al. (1999) who studied the heat transfer from catalyst spheres, Nijemeisland and Dixon (2004) who investigated the heat transfer in a fixed bed of spheres, and Gan et al. (2003) who simulated the sedimentation of solid particles with thermal convection. The last study used the arbitrary Lagrangian–Eulerian (ALE) finite element method (FEM).

The inherent disadvantage of re-meshing and ensuring for an adequate number of interparticle nodes has motivated researchers to use non-fitted methods, such as the Lattice Boltzmann or the Immersed Boundary Methods, which are examined in Sects. 2.5.3 and 2.5.4.

2.5.2 *The Front-Tracking Method*

The introduction of the Front-Tracking Method (FTM) for the solution of particulate flow problems started with the work of Marshall (1986), who solved the Stefan problem using this method. He formulated the Stefan problem as an ordinary differential equation, initial-value problem for the moving boundary coupled with a parabolic partial differential equation for the temperature field. The numerical calculations gave excellent results for the one-dimensional propagation of the solid front with straight and curved moving boundaries. Unverdi and Tryggvason (1992) extended the FTM to particulate and bubbly flows in viscous fluids.

The FTM avoids an implicit interface description within the carrier fluid domain. Such a description requires grid reconstruction at each time step to estimate the position and slope of the interface. Instead, the method uses a different grid on the interface surface, which is distinct from the grid of the flow domain. The second grid requires restructuring because the interface moves and deforms continuously as the calculations progress in time. Unverdi and Tryggvason (1992) discretized the carrier flow field by a finite difference approximation on a stationary cubical grid and used a two-dimensional triangular grid for the interface. The interface points are sometimes called the "marker points." Given the front location, the Eulerian marker function field as well as the corresponding density, viscosity, and force due to surface tension are determined and are used to calculate the solution, from which the Lagrangian points of the interface are advected. The FTM introduces a natural way to accommodate surface tension effects and other forces that determine the surface deformation. The method also keeps the density and viscosity stratification sharp.

An advantage of the FTM is that the unit outward normal on the interface may be directly obtained from the Lagrangian surface/front grid. This is accomplished by relating the grid gradient to a sum of the projections of the Lagrangian grid points, which define the interface:

$$\nabla F_Z(x_i) = \sum_{k=1}^{N_i} Z\vec{n}_j \delta A_j, \tag{2.44}$$

where F_Z is the function that defines the front at the Eulerian grid points x_i and n_j is the normal vector to the elemental area δA_j of the front. This procedure results in the solution of a Poisson equation that solves for the "marker function," which defines the marker points:

$$\nabla^2 F_Z = \vec{\nabla} \cdot \left(\vec{\nabla} F_Z \right). \tag{2.45}$$

Once the marker function and the marker points are known at a given time step, the density and effective viscosity of the Eulerian field are computed, and the computations for the carrier fluid and the interface proceed to the next step. Because volume is not explicitly preserved, renormalization is required to ensure the volume conservation at the interface. Tryggvason et al. (2001) extended the FTM and performed DNS of multiphase flows. They discussed the problem of the moving interface as well as the transfer of information between the moving front grid and the fixed Eulerian grid. They also gave examples of the application of the FTM to homogeneous bubbly flows, atomization, flows with variable surface tension, solidification, and boiling.

2.5.3 The Lattice Boltzmann Method

The Lattice Boltzmann Method (LBM) was developed in the 1990s and is based on statistical mechanics (Frisch et al. 1986, 1987). The flow field is modeled by a system of nodes (fluid particles), typically in a square or cubic arrangement. A distribution function, $f_i(x,t)$, and its evolution, $f_i(x+u_i\Delta t,t+\Delta t)$ which describes the interaction and evolution of the fluid nodes, is defined as follows:

$$f_i(\vec{x}+\vec{u}_i\Delta t, t+\Delta t) = f_i(\vec{x},t) - \frac{f_i(\vec{x},t) - f_i^{\mathrm{eq}}(\vec{x},t)}{\tau}, \tag{2.46}$$

where $f_i^{\mathrm{eq}}(x,t)$ is the well-defined equilibrium state of the distribution function and τ is the dimensionless relaxation time. When the latter is defined in terms of the dimensionless viscosity as

$$v^* = (2\tau - 1)/6, \tag{2.47}$$

it has been proven that the LBM method models a viscous fluid with kinematic viscosity, v, and that the computational error from this modeling is related to the characteristic speed of the flow, U_c; the grid timescale, Δt; and the grid spacing, Δx, through a computational Mach number, Ma. The latter is defined as

$$Ma \equiv \frac{U_c}{\frac{\Delta t}{\Delta x}} = \frac{U_c \Delta x}{v}\left(\frac{2\tau - 1}{6}\right), \tag{2.48}$$

where v is the actual viscosity of the fluid. When $Ma \ll 1$, the LBM describes accurately the viscous flow (Ladd 1994a). The equilibrium distribution function for a viscous fluid is given by the expression:

$$f_i^{\mathrm{eq}}(\vec{x},t) = \rho w_i \left[1 + 3\vec{e}_i \cdot \vec{u} + \frac{9}{2}(\vec{e}_i \cdot \vec{u})^2 - \frac{3}{2}\vec{u} \cdot \vec{u}\right]. \tag{2.49}$$

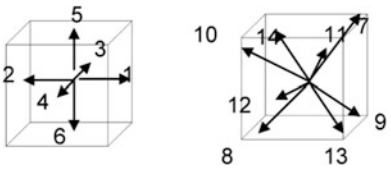

Fig. 2.12 The 14 interactions of the node at the center of the cube with nodes at the vertices and faces of the cube. The 15th interaction is the null vector

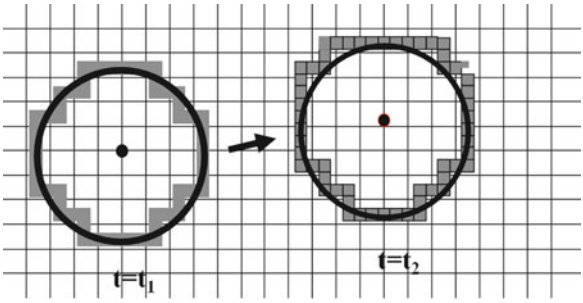

Fig. 2.13 The circular particle, in *black color*, and its surface nodes, in *gray*, at two different times

The weights w_i are well-defined constants in two and three dimensions, and the unit vectors, $\vec{e}_i$, define the ways of interaction of the fluid particles/nodes with their neighboring nodes. In the LBM method, a node is linked only to its surrounding nodes. Figure 2.12 shows the interaction links of the central node in the cube. Interactions in 15 directions are allowed, which means that the central node interacts with other nodes at the centers of the eight vertices of the cube and with the centers of the six faces of the cube. The 15th interaction is covered by the null vector, which implies that the fluid in the central node is at rest, that is, the node interacts with itself only.

In order to describe a surface, Ladd (1994a, b) and Ladd and Verberg (2001) introduced the *bounce-back rule*, which defines a surface in the LBM: According to this rule, the particle surface is represented by the so-called *boundary nodes*. The boundary nodes are a set of the midpoints of the links between two fixed grid nodes. One of the boundary nodes is within the fluid domain, and the other is within the domain of the solid particle. Figure 2.13 shows the surface boundary nodes, in gray color, for a circular particle, in solid black color, within a rectangular grid at two different times. The interactions at the boundary nodes are prescribed in a way to fulfill the zero penetration and the no-slip condition at this boundary (Ladd 1994b). The simplest way to achieve the boundary conditions is to reflect (bounce back) all the interactions and fluid elements on the boundary surface. This condition is satisfied if all the fluid elements that are directed from the fluid domain to the surface are canceled by the corresponding fluid elements emanating from the interior of the solid domain and are directed to the surface of the particle:

$$f_i^{\text{in}}(\vec{x}) = f_i^{\text{out}}(\vec{x}). \tag{2.50}$$

The application of this rather simple condition at the boundary nodes ensures the complete reflection of the fluid elements on the "surface" and the de facto application of the no-penetration and no-slip conditions. If necessary, it is possible to modify the bounce-back rule and to allow partial interaction at the interface, so that partial penetration and partial slip are allowed, as in the case of a porous boundary (Walsh et al. 2009).

The definition of particle boundaries introduces significant problems with the use of the LBM: At first, the numerical scheme makes it necessary to use a large number of lattice grids for every particle in the flow field if the physical boundaries are to be represented accurately. This necessitates a very dense grid for particles with irregular shapes. Secondly, the finite number of boundary nodes makes necessary the stepwise representation of the particle boundary. This causes fluctuations on the computation of the hydrodynamic force acting on the particle and limits the ability of the LBM to solve particle–fluid interaction problems at high Reynolds numbers. Thirdly, when a particle moves, its computational boundary changes and may vary significantly between time steps. This is apparent in Fig. 2.12, which shows that the "particle" as described by its own surface, in gray, has changed shape between the times t_1 and t_2. The surface modification after each time step causes fluctuations in the computation of forces and velocities of the particle. Several authors have used the matching of empirical, closure expressions for the drag coefficient of particles to make the shape transition smoother and to ensure that the actual computational scheme does not become unstable.

Another, but rather minor, problem associated with the application of the LBM is that the bounce-back rule treats the particle–fluid interaction only at the surface of the particle. The interior of the particle domain remains "fluid" during the computations. Thus, the rigid body motion in the interior of the particle is not a priori enforced. The problem that is actually solved by the LBM is the interaction between a fluid and a solid shell, which has a similar boundary as the particle and carries the entire mass of the particle. The contribution of the particle interior to the particle motion and fluid–particle interactions is ignored. It is fortuitous that the effect of the interior fluid is not significant in the hydrodynamic interactions of the solid particles. This was proven by Ladd and Verberg (2001) who showed that accurate computations may be carried out with or without considering the interior fluid.

2.5.4 The Immersed Boundary Method

The Immersed Boundary Method (IBM) was first developed by Peskin (1977) to model the motion of the moving boundary of the human heart. Fogelson and Peskin (1988) have showed that this method could also be employed to simulate flows with suspended, deformable, or rigid particles. Glowinski et al. (2001) assisted in the

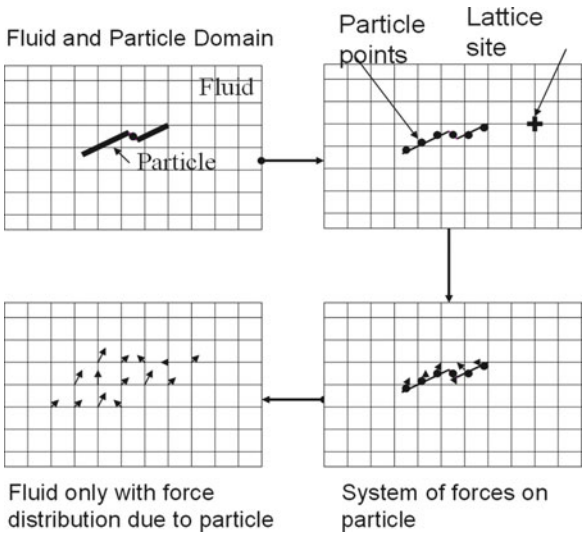

Fig. 2.14 The four stages in the conceptual development of the IBM

development of the IBM by using Lagrange multipliers and the fictitious domain method (FDM) to enforce the no-slip boundary condition at the fluid–particle interface. Feng and Michaelides (2004) combined the IBM and the LBM by computing the force density through a penalty method in the simulations of particulate flows.

The IBM uses a fixed Cartesian mesh for the fluid, which is composed of Eulerian nodes. For the solid boundaries that are immersed in the fluid, the IBM uses a set of Lagrangian boundary nodes, which are advected by the fluid–particle interactions. It may be said that the IBM uses two computational domains: one for the fluid and one for the particulate phase. The interactions between the two domains emanate from the application of a suitable system of forces on the Eulerian fluid domain.

Feng and Michaelides (2005) extended the IBM and developed the *Proteus* numerical code, which incorporates a fictitious domain method and a direct forcing scheme to model the flow of very large numbers of particles in two and three dimensions. Shortly afterward, Uhlmann (2005) independently developed a similar numerical method. The main advantage of these two methods is that the force term is not obtained by a feedback mechanism but by a direct numerical approach. The final result on the computations is that oscillations due to the fixed grid are suppressed because the methods have the ability to smoothly transfer variables between the Lagrangian and Eulerian domains. Another advantage of the IBM is the direct and explicit formulation of the fluid–solid interaction force. Because of this, the IBM with direct forcing produces weaker artificial oscillatory transient particle forces than other methods and has resulted in higher computational efficiency and accuracy compared to the indirect methods.

Figure 2.14 depicts the conceptual design of the IBM, with the four diagrams showing the stages of the development of the numerical scheme. The arrows

connecting the four diagrams follow the development of the method. A particle, which may be rigid or deformable, is in the domain of the carrier fluid, and a Eulerian numerical grid is applied to the entire fluid–particle domain. In the first diagram of the figure, the particle appears as a fiber that may be deformable or rigid.

In the second stage of the method, the surface of the particle is discretized by a number of surface points. The number of the points chosen must be sufficient to describe the surface of the particle within the required degree of accuracy. It must be noted that a more accurate representation of deformable particles requires a higher number of surface points as well as the accurate description of the forces that resist the deformation, e.g., surface tension forces or chemical bonds. A system of springs is chosen to connect each surface point with its neighbors, and the stiffness (spring constant) of the springs will determine the deformation of the surface. For example, very high stiffness will result in rigid particles, while low stiffness results in easily deformable particles.

The third stage in the application of the method determines the system of the hydrodynamic forces acting on the surface of the particle and applies them on the points that represent the surface of the particle. Since the surface points do not coincide with the fluid lattice points, this system of forces is appropriately transposed on the fluid lattice points that are neighbors to the particle surface points.

The transposition of the forces is the fourth stage of the IBM and is shown schematically in the fourth diagram of Fig. 2.14. The net effect, which is apparent between stages 1 and 4 and which defines the IBM, is the substitution of the surface of the particle by an equivalent system of forces, which has the same effect on the fluid as the surface of the particle. Hence, the Navier–Stokes equations for the fluid domain include an additional force, $\vec{f}$, which is due to the presence of the particle:

$$\rho_{\mathrm{f}}\left(\frac{\partial \vec{u}}{\partial t}+\vec{u}\cdot\nabla\vec{u}\right)=\mu\nabla^2\vec{u}-\vec{\nabla}P+\vec{f}. \tag{2.51}$$

This force vanishes at the fluid lattice sites that do not neighbor the particle surface points. The no-slip boundary condition at the interface is automatically satisfied by enforcing the velocity at all boundaries to be equal to the velocity of the fluid at the same location:

$$\frac{\partial \vec{X}(s,t)}{\partial t}=\vec{u}(X(s,t),t), \tag{2.52}$$

where s is the parameter that represents the points on the surface of the particle, and $x = X(s,t)$ is the representation of the particle surface function in the Eulerian domain. Surface slip and penetrating conditions may also be prescribed by modifying Eq. (2.52).

2.5.5 Application of the IBM to Heat Transfer

Particulate heat transfer may also be studied directly using the IBM. For the computation of the heat transfer, Yu et al. (2006) employed the fictitious domain method to study two-dimensional particulate flow with heat convection. They used Lagrangian multipliers to resolve the heat interactions between the fluid and particles. Kim and Choi (2004) used a version of the IBM to study heat transfer problems with stationary particles and complex geometries. Also Pacheco et al. (2005) presented an IBM based on the finite-volume method to study the heat transfer and fluid flow problems with non-staggered grids.

Feng and Michaelides (2008, 2009) extended the IBM in a straightforward and direct way to apply to the energy equation. They introduced an approach that utilizes the main premise of the IBM for the solution of the energy interaction between particles and fluid. According to this approach, the modified momentum and energy equations are solved only on the Eulerian grid. This provides a simplification for the overall numerical technique and requires significantly lower computational resources and CPU time. They postulated that the surface of particles, which exchange thermal energy with the fluid, may be substituted by a system of discretized heat sources and sinks. The net effect of this system of heat sources and sinks on the fluid is to exchange the same amount of heat between the particles and the fluid. Thus, the energy equation for the fluid is modified to include the heat sources that represent the particles as follows:

$$\rho_f c_f \frac{\partial T}{\partial t} + \rho_f c_f \vec{u} \bullet \nabla T = k_f \nabla^2 T + q_{int} + q_{sur}, \tag{2.53}$$

where q_{sur} is the heat that is exchanged due to the heat sources and sinks at the surface of the particle and q_{int} represents any other internal heat sources the fluid may have. The former is the result of the application of the IBM on the energy equation for the fluid–particle system. The heat sources and sinks may be placed on the same boundary nodes where the IBM forces act by a similar transposition technique. Hence, the same point discretization scheme may be used for the momentum and the energy equations, a fact that significantly simplifies the computational method and accelerates the computations.

The IBM is ideally suited for the simulation of the effects of deformed immersed boundaries and has been widely used in biological fluid dynamics. The method is robust and may handle very large numbers of interacting and deformable particles, such as biological cells. The addition of the capability to model the energy and mass exchange between the fluid and the particles makes it ideally suited for applications where momentum, mass, and energy exchange are important for the modeling of discrete particles, such as blood cells, drug delivery, and fluidized bed reactors.

Bibliography

Ashgriz N, Poo JY (1990) Coalescence and separation in binary collisions of liquid drops. J Fluid Mech 221:183–204

Boure JA, Delhaye J-M (1982) General equations and two-phase modeling. In: Gad H (ed) Handbook of multiphase systems. Hemisphere, New York

Chen S, Doolen GD (1998) Lattice Boltzmann method for fluid flows. Annu Rev Fluid Mech 30:329–364

Crowe CT, Sommerfeld M, Tsuji Y (1998) Multiphase flows with droplets and particles. CRC, Boca Raton, FL

Cundall PA, Strack OD (1979) A discrete numerical model for granular assemblies. Geotechnique 29:47–54

Davis A, Michaelides EE, Feng Z-G (2011) Particle velocity near vertical boundaries – a source of uncertainty in two-fluid models. Powder Technol. doi:10.1016/j.powtec.2011.09.031

Delhaye J-M (1981) Basic equations for two-phase modeling. In: Bergles AE, Collier JG, Delhaye J-M, Hewitt GF, Mayinger F (eds) Two-phase flow and heat transfer in the power and process industries. Hemisphere, New York

Ding J, Gidaspaw D (1990) A bubbling fluidization model using kinetic theory of granular flow. AIChE J 36:523–538

Estrade JP, Carentz H, Laverne G, Biscos Y (1999) Experimental investigation of dynamic binary collision of ethanol droplets—a model for droplet coalescence and bouncing. Int J Heat Fluid Flow 20:486–491

Feng Z-G, Michaelides EE (2001) Heat and mass transfer coefficients of viscous spheres. Int J Heat Mass Transf 44:4445–4454

Feng Z-G, Michaelides EE (2004) An immersed boundary method combined with lattice Boltzmann method for solving fluid and particles interaction problems. J Comput Phys 195:602–628

Feng Z-G, Michaelides EE (2005) Proteus—a direct forcing method in the simulation of particulate flows. J Comput Phys 202:20–51

Feng Z-G, Michaelides EE (2008) Inclusion of heat transfer computations for particle laden flows. Phys Fluids 20:1–10

Feng Z-G, Michaelides EE (2009) Heat transfer in particulate flows with direct numerical simulation (DNS). Int J Heat Mass Transf 52:777–786

Fogelson AL, Peskin CS (1988) A fast numerical method for solving the three-dimensional Stokes equation in the presence of suspended particles. J Comput Phys 79:50–69

Frank T, Schade KP, Petrak D (1993) Numerical simulation and experimental investigation of gas-solid two phase flow in a horizontal channel. Int J Multiphase Flow 19:187–204

Frisch U, Hasslacher B, Pomeau Y (1986) Lattice-gas automata for the Navier-Stokes equations. Phys Rev Lett 56:1505

Frisch U, D'Humiéres D, Hasslacher B, Lallemand P, Pomeau Y, Rivert JP (1987) Lattice-gas hydrodynamics in two and three dimensions. Complex Syst 1:649–707

Gan H, Chang JZ, Howard HH (2003) Direct numerical simulation of the sedimentation of solid particles with thermal convection. J Fluid Mech 481:385–411

Glowinski R, Pan T-W, Hesla TI, Joseph DD, Periaux J (2001) A fictitious domain approach to the direct numerical simulation of incompressible viscous flow past moving rigid bodies: application to particulate flow. J Comput Phys 169:363–426

Gosman AD, Ioannides E (1983) Aspects of computer simulation of liquid-fueled reactors. Energy 7:482–490

Hinze JO (1975) Turbulence. McGraw-Hill, New York

Höfler K, Schwarzer S (2000) Navier-Stokes simulation with constraint forces: finite-difference method for particle-laden flows and complex geometries. Phys Rev E 61:7146–7160

Ishii M (1975) Thermo-fluid dynamic theory of two-phase flows. Eyrolles, Paris

Ishii M (1990) Two-fluid model for two-phase flow. In: Hewitt GF, Delhaye J-M, Zuber N (eds) Multiphase science and technology, vol 5. Hemisphere, New York, pp 1–63
Jenkins JT, Richman MW (1985) Grad's 13-moment system for a dense gas of inelastic spheres. Arch Ration Mech Anal 87:355–377
Kartushinsky A, Michaelides EE (2004) An analytical approach for the closure equations of gas-solid flows with inter-particle collisions. Int J Multiphase Flow 30:159–180
Kim J, Choi H (2004) An immersed-boundary finite-volume method for simulations of heat transfer in complex geometries. Korean Soc Mech Eng Int J 18(6):1026–1035
Kollar LE, Farzaneh M, Karev AR (2005) Modeling droplet collision and coalescence in an icing wind tunnel and the influence of these processes on droplet size distribution. Int J Multiphase Flow 31:69–92
Ladd AJC (1994a) Numerical simulations of particulate suspensions via a discretized Boltzmann equation. Part 1. Theoretical foundation. J Fluid Mech 271:285–310
Ladd AJC (1994b) Numerical simulations of particulate suspensions in a discretized Boltzmann equation Part II. Numerical results. J Fluid Mech 271:311–339
Ladd AJC, Verberg R (2001) Lattice-Boltzmann simulation of particle-fluid suspensions. J Stat Phys 104:1191–1251
Manga M, Stone HA (1993) Buoyancy-driven interactions between two deformable viscous drops. J Fluid Mech 256:647–683
Manga M, Stone HA (1995) Low Reynolds number motion of bubbles, drops and rigid spheres through fluid-fluid interfaces. J Fluid Mech 287:279–298
Marshall G (1986) A front tracking method for one-dimensional moving boundary problems. SIAM J Sci Stat Comput 7:252–263
McKenna TF, Spitz R, Cokljat D (1999) Heat transfer from catalysts with computational fluid dynamics. AIChE J 45:2392–2410
Michaelides EE (2003) Introduction and basic equations for multiphase flow. In: Buchlin J-M (ed) von Karman institute lecture series, 19–23 May 2003, Brussels, Belgium
Michaelides EE, Li L, Lasek A (1992) The effect of turbulence on the phase change of droplets and particles under non-equilibrium conditions. Int J Heat Mass Transf 34:2069–2076
Morioka S, Nakajima T (1987) Modeling of gas and solid particles two-phase flow and application to fluidized bed. J Theor Appl Mech 6:77–88
Mostafa AA, Elghobashi SE (1985) A two-equation turbulence model for jet flows laden with vaporizing droplets. Int J Multiphase Flow 11:515–533
Nijemeisland M, Dixon AG (2004) CFD study of fluid flow and wall heat transfer in a fixed bed of spheres. AIChE J 50:906–921
Nobari MRH, Jan YJ, Tryggvason G (1996) Head on collisions of drops – a numerical investigation. Phys Fluids 8:29–42
Orme M (1997) Experiments on droplet collisions bounce, coalescence and disruption. Prog Energy Combust Sci 23:65–79
Pacheco JR, Pacheco-Vega A, Rodic T, Peck RE (2005) Numerical simulations of heat transfer and fluid problems using an immersed-boundary finite-volume method on non-staggered grids. Numer Heat Transf B 48:1–24
Patankar N, Ko T, Choi HG, Joseph DD (2001) A correlation for the lift-off of many particles in plane Poiseuille flows of Newtonian fluids. J Fluid Mech 445:55–76
Peskin CS (1977) Numerical analysis of blood flow in the heart. J Comput Phys 25:220–252
Peskin CS (2002) The immersed boundary method. Acta Numer 11:479–517
Piomelli U, Balaras E (2002) Wall-layer models for large-eddy simulations. Annu Rev Fluid Mech 34:349–374
Qian J, Law CK (1997) Regimes of coalescence and separation in droplet collisions. J Fluid Mech 331:59–80
Reeks MW (1991) On a kinetic equation for the transport of particles in turbulent flows. Phys Fluids 3:446–456

Reeks MW, Simonin O (2006) PDF models. In: Multiphase flow handbook, sect. 13.4.3. CRC, Boca Raton, FL, pp 13-89–13-113

Sakiz M, Simonin O (1999) Development and validation of continuum particle wall boundary conditions using Lagrangian simulations of a vertical gas-solids channel flow. In: Proceedings of 3rd ASME-JSME joint fluids engineering conference, San Francisco, CA

Simonin O (2001) Statistical and continuum modeling of turbulent reactive particulate flows- Part I: Theoretical derivation of dispersed phase Eulerian modeling from probability density function kinetic equation. In: Buchlin J-M (ed) von Karman institute lecture series. Buchlin, Brussels

Sirignano WA (1999) Fluid dynamics and transport of droplets and sprays. Cambridge University Press, Cambridge

Smagorinsky J (1963) General circulation experiments with the primitive equations, I. The basic experiment. Mon Weather Rev 91:99–152

Sommerfeld M (2003) Analysis of collision effects for turbulent gas-particle flow in a horizontal channel: Part I. Particle transport. Int J Multiphase Flow 29:675–699

Sommerfeld M, Huber N (1999) Experimental analysis and modelling of particle-wall collisions. Int J Multiphase Flow 25:1457–1489

Taniere A, Khalij M, Oesterle B (2004) Focus on the disperse phase boundary conditions at the wall for irregular particle bouncing. Int J Multiphase Flow 30:675–699

Thompson JF, Warsi ZUA, Mastin CW (1982) Boundary-fitted coordinate systems for numerical solution of partial differential equations—a review. J Comput Phys 47:1–108

Tryggvason G, Bunner B, Esmaeeli A, Juric D, Al-Rawahi N, Tauber W, Han J, Nas S, Jan Y-J (2001) A front-tracking method for the computations of multiphase flow. J Comput Phys 169:708–759

Tsuji Y, Kawaguchi T, Tanaka T (1993) Discrete particle simulation in a two dimensional fluidized bed. Powder Technol 77:79–86

Uhlmann M (2005) An immersed boundary method with direct forcing for the simulation of particulate flows. J Comput Phys 209:448–476

Unverdi SO, Tryggvason G (1992) A front-tracking method for viscous, incompressible, multi-fluid flows. J Comput Phys 100:25–37

Wallis GB (1963) Some hydrodynamic aspects of two-phase flow and boiling. In: International developments in heat transfer. ASME, New York

Walsh STC, Burnwinkle H, Saar MO (2009) A new partial-bounce back lattice-Boltzmann method for fluid flow through heterogeneous media. Comput Geosci 35:1186–1193

Warsi ZUA (1993) Fluid dynamics: theoretical and computational approaches. CRC, Boca Raton, FL

Yu Z, Shao X, Wachs A (2006) A fictitious domain method for particulate flows with heat transfer. J Comput Phys 217:424–452

Zaichik LI, Vinberg AA (1991) Modeling of particle dynamics and heat transfer in turbulent flows using equations for first and second moments of velocity and temperature fluctuations. In: Proceedings of 8th international symposium on turbulent shear flows, Munich, FRG, vol 1, pp 1021–1026